Economic Geology
Vol. 98, 2003, pp. 1107–1135

Geology and Geochemistry of the Deep Star Gold Deposit, Carlin Trend, Nevada

DEAN G. HEITT,† W. WARREN DUNBAR,
Newmont Mining Corporation, P.O. Box 669, Carlin, Nevada 89822

TOMMY B. THOMPSON,
Center for Research in Economic Geology, Mail Stop 169, Mackay School of Mines, University of Nevada-Reno, Reno, Nevada 89557

AND ROBERT G. JACKSON
150 East Flora Lane, Spring Creek, Nevada 89815

Abstract

Deep Star is a high-grade Carlin-type gold deposit located in the northern part of the Carlin trend. The deposit averages 34.0 g/t Au and by year end 2000 had produced 37.8 t (1,217,000 oz) gold with a remaining reserve of 16.0 t (513,698 oz) gold. The deposit is primarily hosted in brecciated calc-silicate rocks of the Devonian Popovich Formation, with a minor amount of gold in the Jurassic Goldstrike diorite. Intrusion of the syn- and postore Deep Star rhyolite constrains the age of the mineralization. The postore rhyolite is compositionally and mineralogically similar to the synore dike and yielded an average $^{40}Ar/^{39}Ar$ isochron age of 38.3 Ma. Eocene rhyolite dikes intruded active, dilatant north- to northeast-striking faults and/or fractures, providing an important age constraint on the local stress regime at Deep Star during mineralization. Essentially horizontal, west-northwest-directed Eocene extension (291°) is consistent with dextral-normal oblique slip observed on north-south-striking, east-dipping portions of the Gen-Post fault system and dilation and sinistral shear on dike-filled, northeast-striking structures. A right-stepping, releasing bend in the Deep Star fault at its intersection with northwest- and north-northwest-striking subsidiary structures created a deep-tapping dilatant conduit for gold-bearing hydrothermal fluids.

Five stages of hydrothermal alteration are present at Deep Star. Stages 1 and 2 are related to thermal metamorphism, metasomatism, and possibly retrograde alteration associated with intrusion of the Goldstrike stock. Stage 3 consists of preore quartz-carbonate alteration. The carbonate minerals are zoned both laterally and vertically, with dolomite as the dominant mineral closest to ore. Stage 3 overlaps with stage 4 quartz-kaolinite alteration associated with the introduction of gold and is therefore interpreted to be part of the Eocene mineralizing event. Gold is hosted in As-rich rims on marcasite and pyrite within a kaolinite and quartz matrix. Postore stage 5 is dominated by calcite with lesser siderite and barite.

A three-dimensional geochemical model of the Deep Star deposit and its environs reveals that Carlin-type systems may have a geochemical expression involving a much broader suite of elements than previously recognized. Elements with distribution patterns considered to be related to the mineralizing event include Ag, As, Au, Ba, Bi, Ca, Cd, Co, Cu, Fe, Hg, Mg, Mo, Mn, Ni, P, Pb, S, Sb, Se, Te, Tl, U, V, W, and Zn. The multielement anomaly associated with the Deep Star deposit is best described as a vertical plume that is (1) focused between the Deep Star and Post faults below the deposit, (2) present in the footwall of the Deep Star fault and the Deep Star-Post fault corridor at the level of the deposit, and (3) broadly dispersed above, and to the west of, the deposit under the influence of northeast- and northwest-trending structural fabrics. Most closely associated with gold deposition are enrichments in As, Sb, Hg, Tl, Ag, and Zn within a halo of Ca, Mg, Ba, and Sr depletion. The elements Fe, Mn, Co, Ni, and P are most elevated in the immediate hanging wall of the Deep Star fault and above the deposit in a region where secondary carbonate veins (ankerite, kutnahorite, and Mn-rich dolomite); open-space-filling carbonate minerals (siderite, calcite) have been observed. Some lateral zonation is evident at levels above the deposit, with increases of Pb and Bi on its eastern margin and more Mo, U, V, and W west of the deposit.

Isotopic analyses of kaolinite are interpreted to indicate that gold-mineralizing fluids originated from either a magmatic or possibly a deep metamorphic source. Fluids range from near the magmatic water field for those near the center of the Deep Star orebody along a mixing path toward exchanged mid-Tertiary meteoric water as represented by the fluids near the eastern orebody margin.

Introduction

THE CARLIN TREND is a 60-km-long alignment of gold deposits located in northeastern Nevada. The Deep Star deposit is located in the northern part of the Carlin trend, approximately 450 m north of the Genesis-Bluestar mine and 1,525 m south of the Betze-Post mine at latitude 40°57'38" N, longitude 116°21'42" W (Fig. 1). The Carlin trend contains one of the largest concentrations of gold deposits in North America with over 40 deposits of varying size having been discovered to date (Heitt, 2000). Historic production and current reserves exceed 3,110 metric tons (t) of gold (Teal and Jackson, 1997; Heitt, 2000).

Major gold deposits on the Carlin trend are classified as sedimentary rock-hosted disseminated gold, or "Carlin-type" deposits. Radtke and Dickson (1974) defined the term Carlin-type to include deposits that shared similar characteristics

† Corresponding author: e-mail, dhei1@nevada.newmont.com

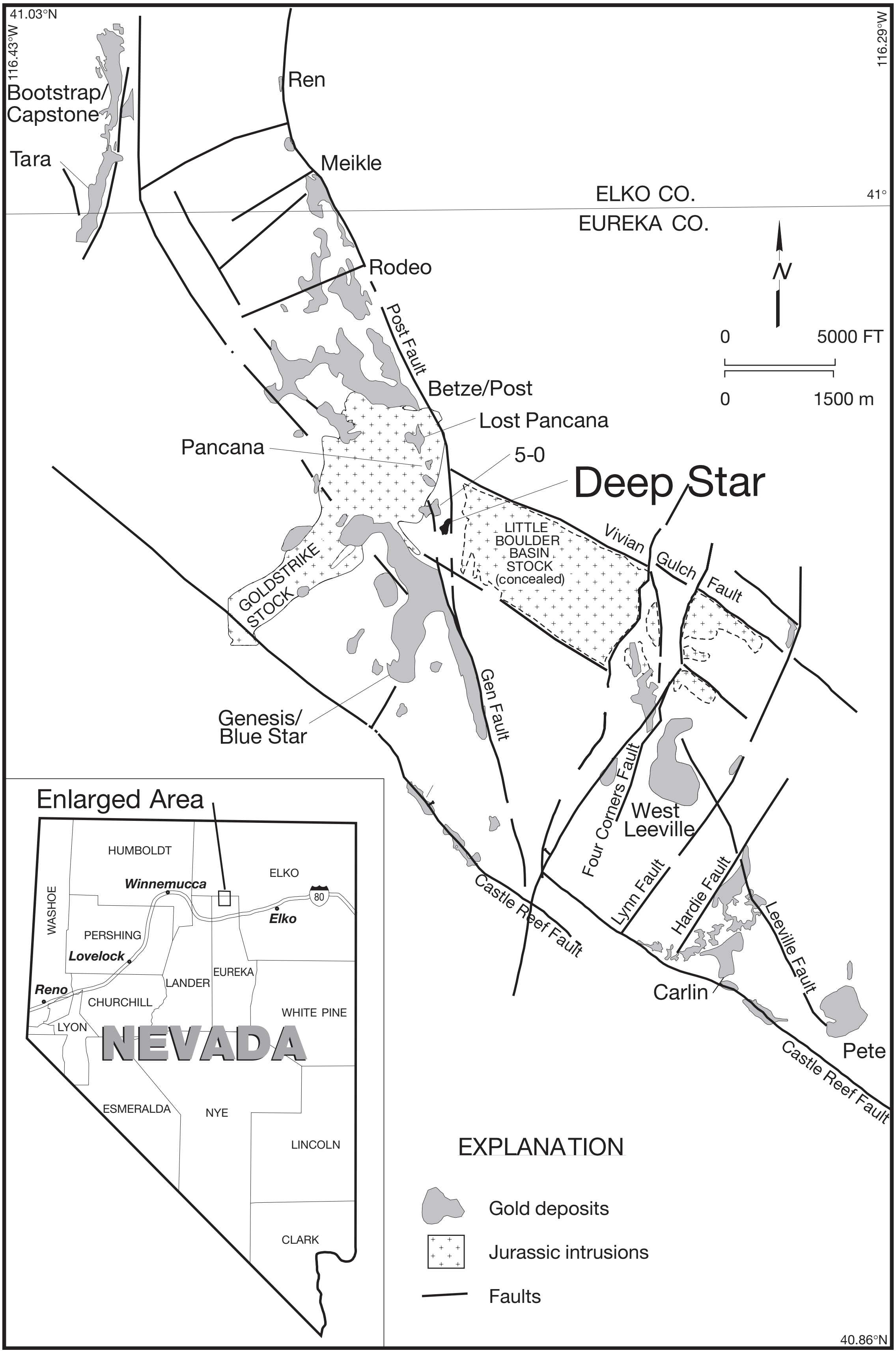

Fig. 1. Location map of the north Carlin trend, Nevada.

such as finely disseminated gold, carbonate host rocks, orebodies conformable to bedding, relatively simple alteration, and other characteristics common to all such deposits known at the time.

Christensen et al. (1987) recognized that although all the Carlin-type deposits on the Carlin trend shared some common attributes, each deposit was unique. They divided the Carlin trend into six subdistricts on the basis of geographic, structural, lithologic, alteration, and geochemical characteristics. Deep Star is located in the Blue Star-Goldstrike subdistrict where a strong structural control to the ore is a characteristic common to all the deposits. Teal and Jackson (1997) attempted to quantify further the controls and styles of mineralization for deposits on the Carlin trend using a four-field classification scheme. In this classification, Deep Star plots near a line defined by breccia as the main style of mineralization and faults and/or folds as the main control to mineralization. Clode et al. (1997) characterized Deep Star as the prime example of the structural end member of Carlin-type deposits. Much effort has been made to study and characterize the structural controls that localized the high-grade ore at Deep Star. This research on the fundamental controls of Deep Star has helped shed light on the differences and similarities between Deep Star and other Carlin-type deposits. This paper combines a description of the deposit from core logging and underground mapping with recent studies of the structural history (Dunbar, 2001), alteration paragenesis by Terry Leach (written commun., 1999, 2000) and Tommy Thompson, trace element geochemistry by Robert Jackson, and new kaolinite δD and $\delta^{18}O$ isotopic data.

Exploration and Discovery

Early exploration in the Genesis-Bluestar and Betze-Post mine areas focused on near-surface oxide gold mineralization. Numerous small deposits were discovered and mined between 1978 and 1986 by Western States Mining including the 5-0 pit (Fig. 1) located 365 m north of Deep Star (Bettles, 1989). Approximately 0.09 t of gold was produced from oxidized, shallow-dipping, quartz-carbonate-filled shear veins in the Goldstrike intrusion. In 1987, Newmont Mining Corporation (Newmont) discovered the near-surface oxide Gold Star prospect hosted by calc-silicate rocks of the Ordovician Vinini Formation south of the Goldstrike stock and inferred a geologic resource of 0.89 t gold averaging 1.37 g/t Au (Robert Ryneer, written commun., 1988). Also in 1987, Barrick Gold Corporation (Barrick) identified a deep exploration target using induced polarization (IP) geophysics (Keith Bettles, written commun., 1993). In September 1988, Barrick discovered the Deep Star deposit when they intersected a 36.6-m mineralized zone grading 8.50 g/t Au starting at 388.6 m (Clode et al., 1997). Newmont offset Barrick's hole in mid-1989, intersecting 59.4 m grading 70.56 g/t Au from 394.7 to 454.2 m. By the end of 1992, Newmont had identified a reserve of 770,213 t grading 31.85 g/t Au for a total of 24.54 t (789,000 oz) of gold (Newmont Gold Company, 1992 Annual Report). In November 1996, Newmont acquired Barrick's portion of the deposit (Newmont Gold Company, Press Release, October 22, 1996).

Production and Reserves

Mine development began in early 1994 with twin parallel, 610-m-long (vent and haulage) declines from the northwest wall of the Genesis open pit. Production began in January of 1996 from upper levels of the orebody using underhand cut-and-fill drifting with cemented backfill. Drift sizes are 3 m wide by 3.6 m high on overcuts and 4.8 m wide by 3.6 m high on undercuts. Production through the end of 2000 totaled 1,019,912 t grading 37.10 g/t Au for a total of 37.8 t (1,216,694 oz) of gold with a remaining reserve at that time of 382,590 t grading 41.76 g/t Au, or 16.0 t (513,698 oz) of gold.

Regional Geologic Setting

The Carlin trend is located along a major crustal break (Rodriguez, 1997) associated with Proterozoic rifting and formation of the continental margin of North America (Wooden et al., 1997). Although no single fault near the surface defines that crustal break, the ore deposits are within favorable host rocks adjacent to structures that extend parallel to and above the crustal break.

Deep Star is situated within a complex zone of lower plate miogeoclinal rocks that have been overthrust by allochthonous eugeoclinal rocks during the Late Devonian to Early Mississippian Antler orogeny (Roberts et al., 1958; Roberts, 1960). The Deep Star orebody is hosted within silty, carbonaceous carbonate rocks beneath the Roberts Mountains thrust (RMT) formed during the Antler orogeny. Subsequent orogenic shortening during the Pennsylvanian and Permian (Humboldt disturbance; Ketner, 1977), Early Triassic (Sonoma orogeny; Silberling and Roberts, 1962), Middle Jurassic (Elko orogeny; Thorman et al., 1990), and Early Cretaceous (Sevier orogeny; Armstrong, 1968) reactivated earlier basement and Antler-related faults. The Jurassic diorite to granodiorite Goldstrike stock and sill complex (Fig. 2) was emplaced during the latter part of the Elko orogeny (Thorman et al., 2000). A metamorphic aureole was formed during intrusion of the stock-sill complex, and the Deep Star mine is wholly within the southeastern perimeter of this aureole.

Magmatism began again during the Cenozoic with emplacement of dacitic to rhyolitic dikes and sills between 40 and 36 Ma (Arehart et al., 1993a; Ressel et al., 2000). These dikes typically strike north-south to northeast through the surface and mine exposures. The Deep Star rhyolite is the youngest set of dikes and sills in the mine area and has both syn- and postore emplacement relations.

A regional north- to north-northwest-striking fault zone (Gen-Post fault system) is the principal control on the localization of ore at Deep Star. Many other orebodies along the Carlin trend are present in the footwall of this fault zone north and south of the Deep Star mine (Fig. 1).

Lithology

Lithologic units in the vicinity of Deep Star consist of Ordovician through Devonian sedimentary rocks in the upper and lower plates of the Roberts Mountains thrust. All of these units have undergone metasomatism and contact metamorphism during intrusion of the Jurassic Goldstrike diorite and are cut by both Jurassic lamprophyre (Arehart et al., 1993a; Orobona, 1996) and Eocene rhyolite dikes (Ressel et al.,

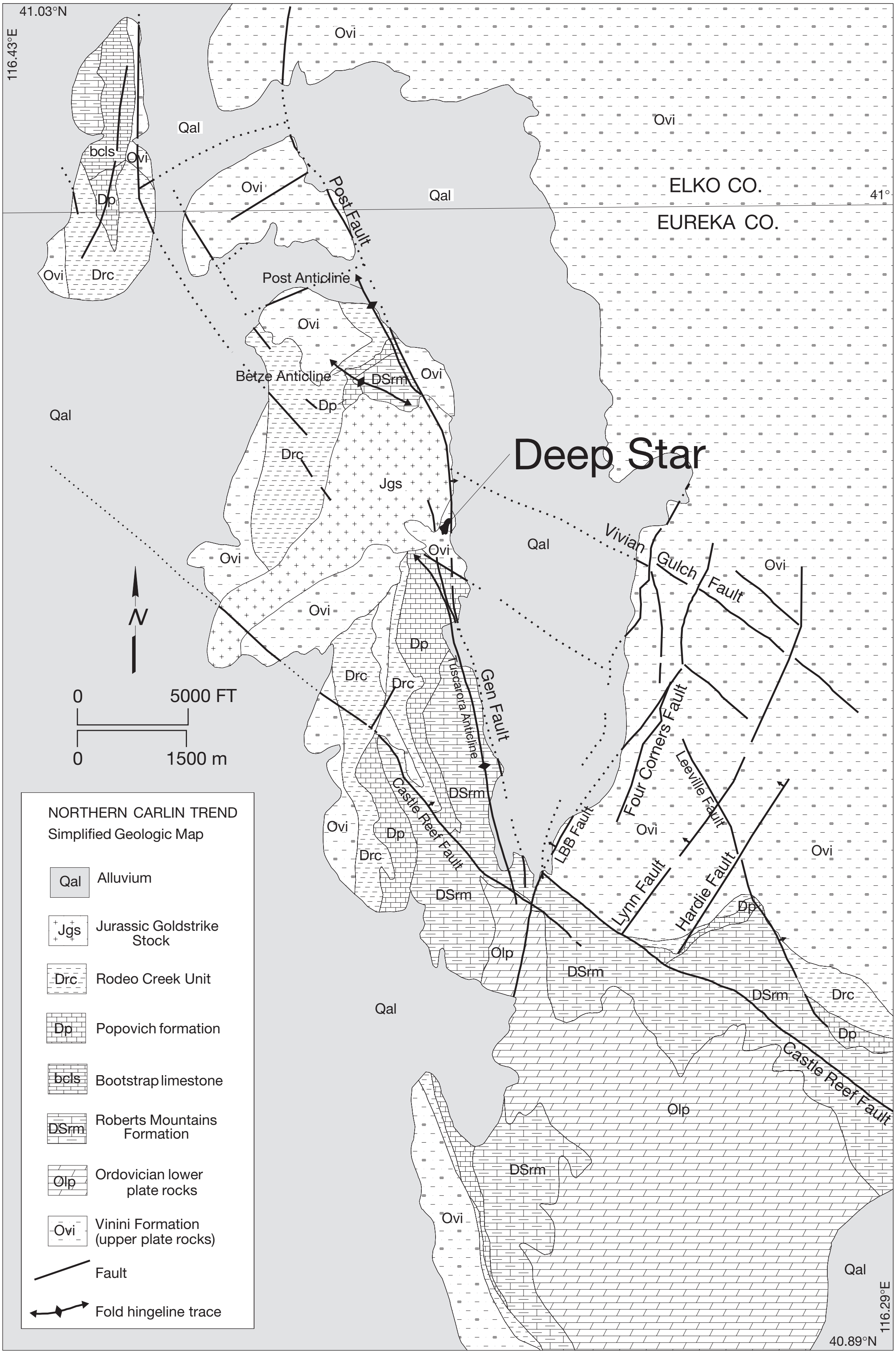

FIG. 2. Simplified geologic map of the north Carlin trend, Nevada. Dotted lines indicate covered faults.

2000; this report). The stratigraphy of the Deep Star area is shown in Figure 3. Figures 4 and 5 show the geology of the immediate mine area in plan and cross sectional views, respectively.

Upper plate

Ordovician Vinini Formation (Ov) forms the upper plate of the Roberts Mountains thrust at Deep Star and consists of thin- to medium-bedded quartz hornfels, metaquartzite, and lesser calc-silicate near the base of the unit. Colors range from pale green to light to medium gray or tan when fresh and yellow-brown when oxidized. Contractional deformation produced thrusting and a penetrative shear fabric that is enhanced by the metamorphism and locally referred to as "flaser texture." The Vinini Formation is estimated to range from 122 to 305 m in thickness, but the lower contact of the unit is truncated by the Roberts Mountains thrust resulting in interleaved thrust slices of the Vinini and underlying Popovich Formations. Sills of the Goldstrike stock have been emplaced along the Roberts Mountains thrust (Figs. 3 and 5).

Lower plate

Devonian Popovich Formation (Dp) and the Silurian-Devonian Roberts Mountains Formation (DSrm) make up the footwall of the Roberts Mountains thrust at Deep Star (Fig. 3). Metasomatism and metamorphism of the rocks at Deep Star render identification of the units making up these formations difficult locally because many textures used to identify them elsewhere on the Carlin trend are obscured. The Popovich Formation at Deep Star is subdivided into two units (Dp1 and Dp2; upper and lower, respectively) and the Roberts Mountains Formation into four units (DSrm1 through 4, from top to bottom; Fig. 3).

Devonian Popovich Formation (Dp): The upper Popovich Formation unit (Dp1) includes fine-grained diopside calc-silicate rocks, coarse-grained skarn, coarse-grained marble, and minor weakly metamorphosed micrite and phlogopite hornfels. Colors range from light gray to purple-gray, pale green, light brown, or black depending on the degree of metamorphism. Planar-laminated bedding ranges from thin to thick bedded in the calc-silicates and micrite, to massive in the skarn and marble. Contorted bedding related to soft-sediment deformation is common in the micritic units and locally observed in the calc-silicate beds. Locally, elongated angular clasts give the rock a pseudoboudinage texture. This deformation appears to be premetamorphism since calc-silicate assemblages locally overprint the texture. The calc-silicate rocks are made up principally of quartz, diopside, and calcite ± hedenbergite. Skarns are composed of diopside, wollastonite, grossularite, quartz ± calcite ± hedenbergite, phlogopite, and K feldspar. Interbedded coarse-grained marble is common and ranges from less than 2.5 cm to greater than 3 m in thickness, with most units less than 0.5 to 1 m thick. The upper Popovich Formation unit is 122 to 155 m thick.

The lower Popovich Formation unit (Dp2) is dominantly planar-laminated phlogopite hornfels with minor calc-silicate. Lithologies in it have a mineralogy similar to comparable lithologies in the upper Popovich Formation. Colors range from light brown to black. Diagnostic interbedded, calcareous siltstone is altered to light-gray calc-silicate and ranges from 0.6 to 1 cm thick. The lower Popovich Formation unit is moderately to strongly calcareous, especially in the phlogopite beds, and is 9 to 15 m thick.

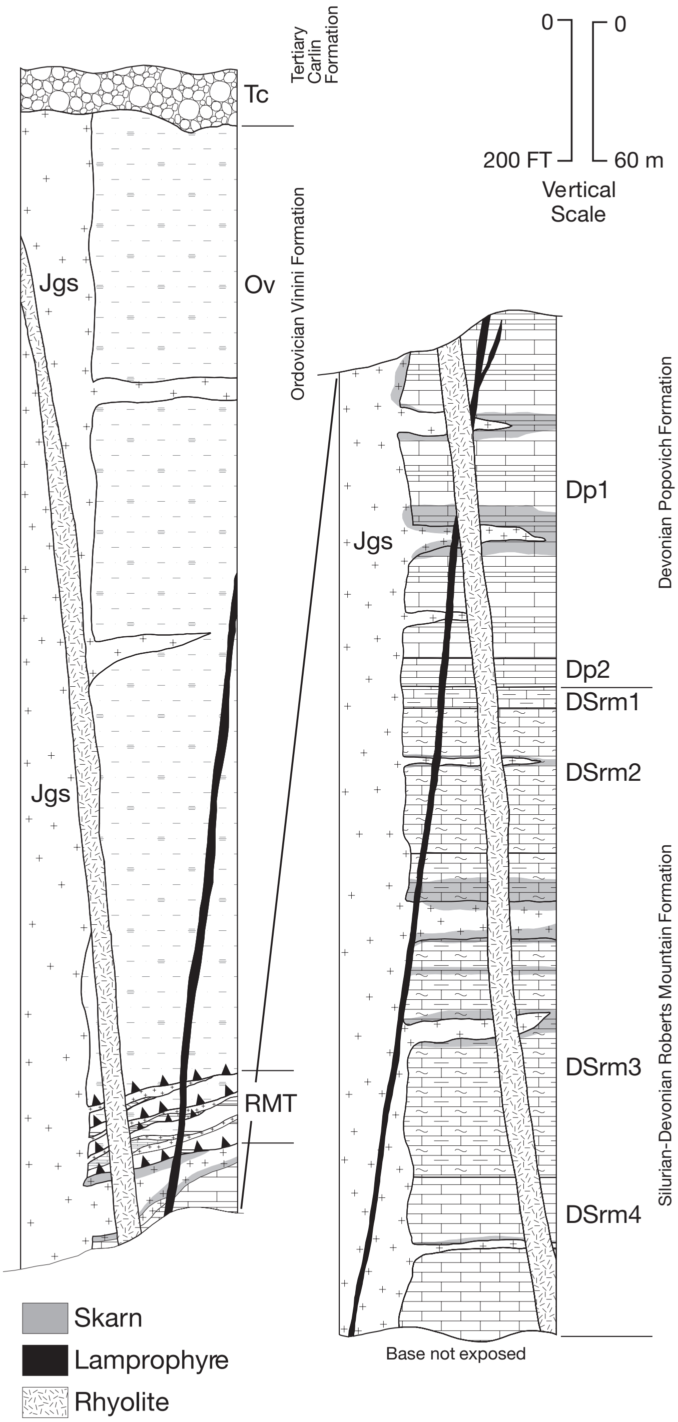

FIG. 3. Stratigraphic column of the Deep Star area, Nevada. See text for detailed descriptions of the stratigraphic units, intrusive rocks, and abbreviations.

Silurian-Devonian Roberts Mountains Formation (DSrm): Unit DSrm1 is the uppermost unit in the formation (Fig. 3). It is characterized by interbedded, planar- and wispy-laminated,

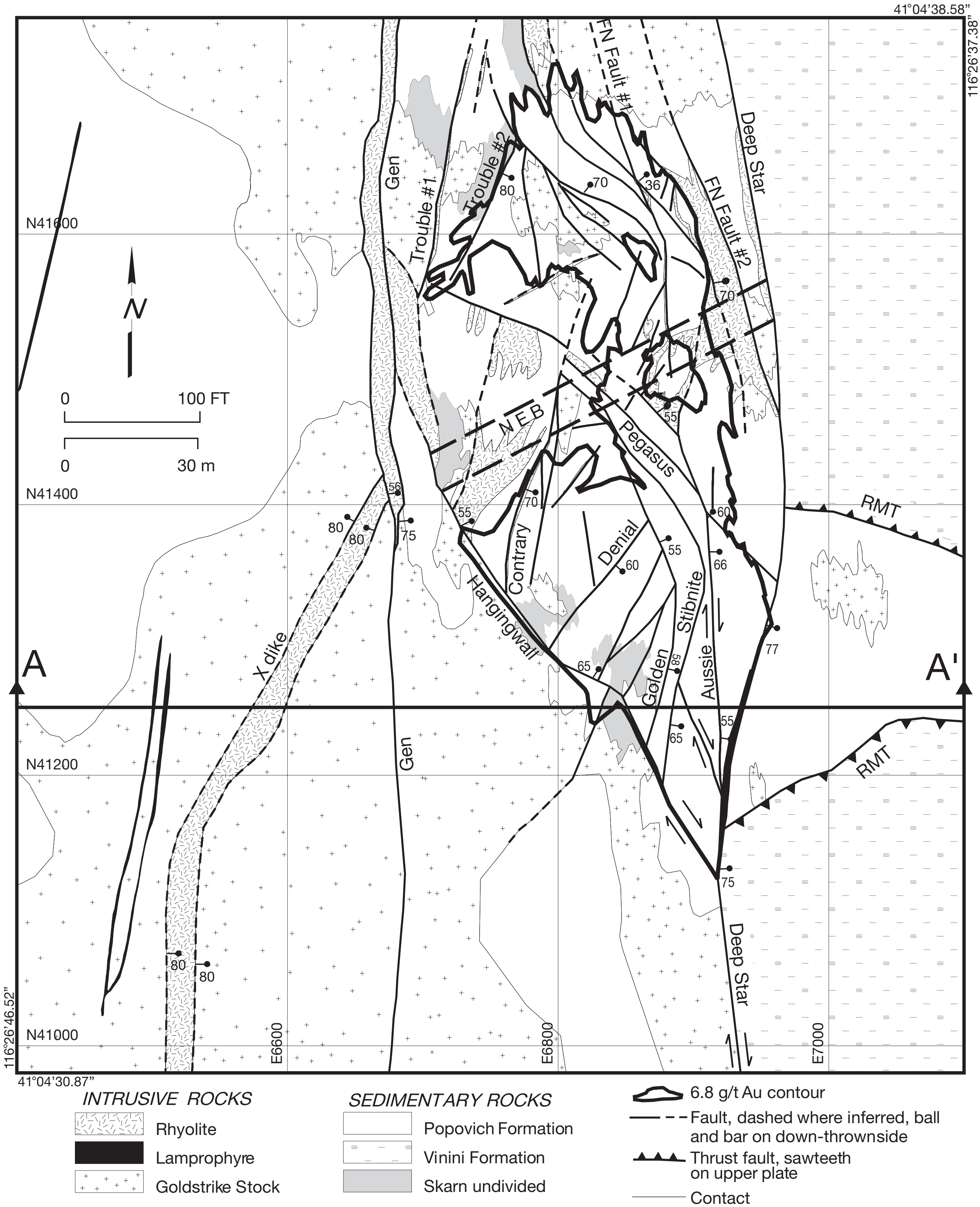

FIG. 4. Interpretive geologic map of the 4570 A level, Deep Star deposit, Nevada. Based on underground mapping and core drilling. A-A', location of the N41250 geologic cross section (Fig. 5). Local mine grid is in feet.

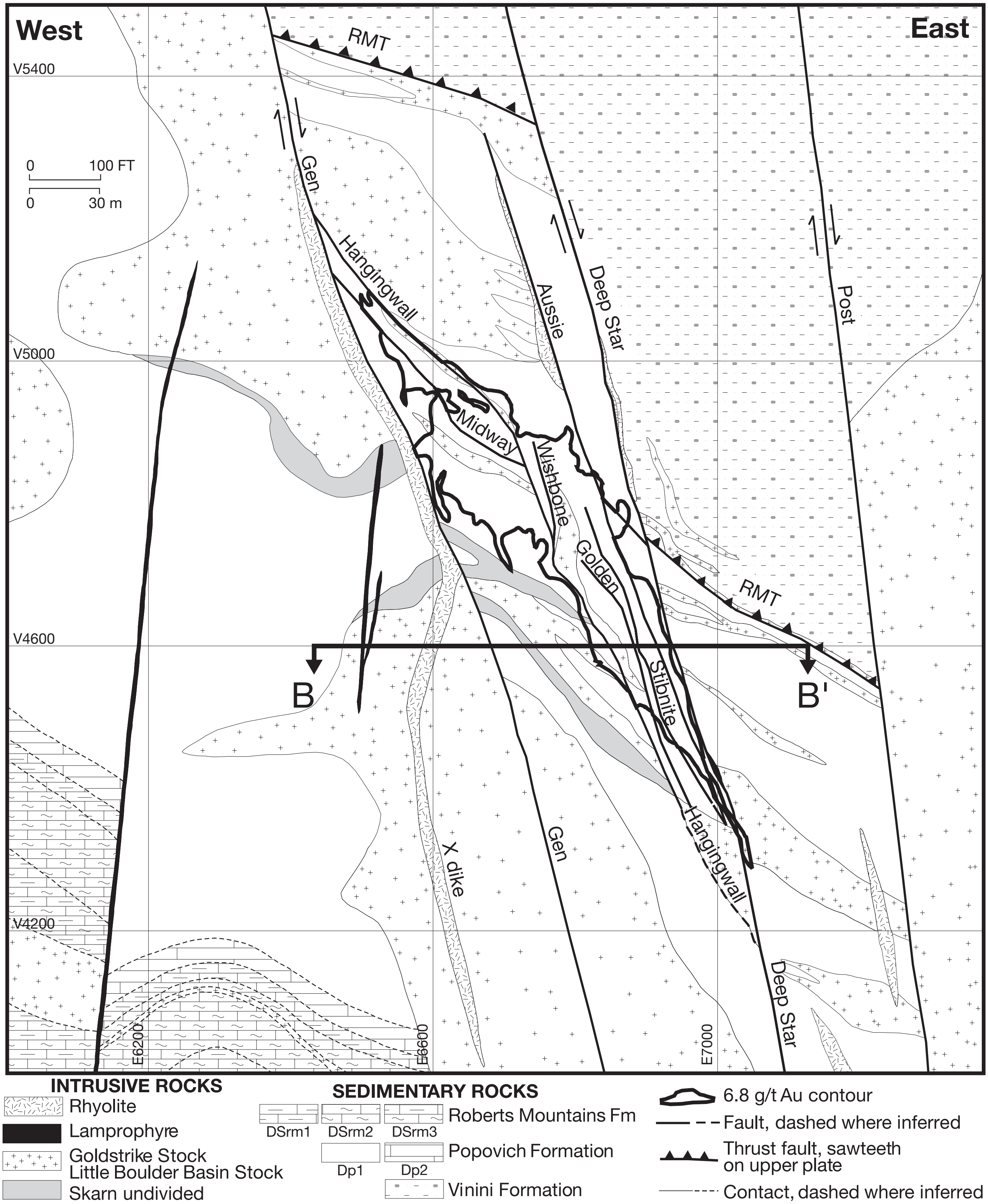

FIG. 5. Interpretive geologic cross section N41250, based on underground mapping and core drilling, Deep Star deposit, Nevada. B- B', location of the 4570 A level geologic map (Fig. 4). Local mine grid and elevations are in feet.

calcareous, phlogopite hornfels and is transitional from the massive or planar-laminated units above to the wispy-laminated units below. "Wispy laminations" refer to a wavy, lens-like mottling interpreted to result from intense bioturbation. Thin calcareous siltstone beds are altered to calc-silicate or marble; relict burrows are diagnostic of this unit. Colors range from light brown to light gray. Unit Dsrm1 is 6 to 9 m thick.

Unit DSrm2 is a thick-bedded, wispy-laminated, calcareous, phlogopite hornfels with minor marble beds. Metamorphism of the wispy laminations imparts a strongly mottled texture. The absence of planar-laminated bedding and the appearance of 5- to 60-cm-thick marble beds mark the contact with the overlying DSrm1. Colors are typically light brown to light gray. The unit is 27 to 34 m thick and is the most easily recognized unit in the metamorphosed section, making it a good marker horizon.

Unit DSrm3 consists of wispy-laminated, calcareous, phlogopite hornfels, marble, coarse-grained skarn, and lesser calc-silicate rock. A 0.6- to 10-m-thick marble bed and a general increase in marble content marks the contact with unit DSrm2. The skarn contains diopside, wollastonite, grossularite ± quartz ± calcite and is common throughout the unit where proximal to intrusive rock. Colors range from light brown in the phlogopite-rich beds to pale-blue marble and multicolored skarn. The thickness of unit DSrm3 is at least 107 m.

DSrm4, the lowermost unit (Fig. 3), contains planar-laminated phlogopite hornfels and interbedded calc-silicate rock. Colors range from light green to white or pale brown. Only the upper part of this unit is present in drill core, so the total thickness is unknown, but elsewhere in the northern Carlin trend it is at least 240 m thick.

Intrusive rocks

The Deep Star deposit is located near the southeastern margin of the Jurassic Goldstrike stock (Jgs) (Fig. 2). The stock has a laccolithic geometry with numerous sills and dikes on its margins and is composed of medium- to coarse-grained diorite with lesser granodiorite and gabbro (Arehart, 1993a; Ressel et al., 2000). A 150- by 300-m apophysis of the stock is present on the southwest margin of Deep Star (Figs. 4 and 5) and produced intense thermal metamorphism in the adjacent sedimentary rocks. The covered Little Boulder Basin stock (Jlbb) located east of Deep Star (Fig. 1) is mineralogically and geochemically similar to the Goldstrike stock and is considered to be comagmatic with it; however, the genetic relationship between the two is not yet proven. Isotopic ages for the Goldstrike stock average 158 Ma (Arehart et al., 1993a; Mortensen et al., 2000).

Jurassic lamprophyre dikes fill narrow high-angle faults and/or fractures and cut the sedimentary rocks as well as the Goldstrike diorite. $^{40}Ar/^{39}Ar$ ages for the lamprophyre dikes range from 157.9 ± 0.02 Ma to 165.7 ± 2.4 Ma (Emsbo et al., 1996; M. Farmer, written commun., 1996; Orobona, 1996); however, crosscutting relationships show that the lamprophyre dikes are younger than the Goldstrike stock so dates older than 158 Ma are suspect. Lamprophyre dikes are generally black to dark green with phlogopite or hornblende phenocrysts and minor olivine in an aphanitic groundmass composed of feldspar, phlogopite or hornblende, carbonate minerals, quartz, and apatite. Most lamprophyre dikes at Deep Star are less than 1.5 m thick.

The Deep Star rhyolite is present as dikes and minor sills composed of a 0.3- to 1-m-thick brown, green, and/or red flow-banded glass chill margin and a central mass consisting of spherulitic sanidine and quartz (Fig. 6A, B, C). Commonly,

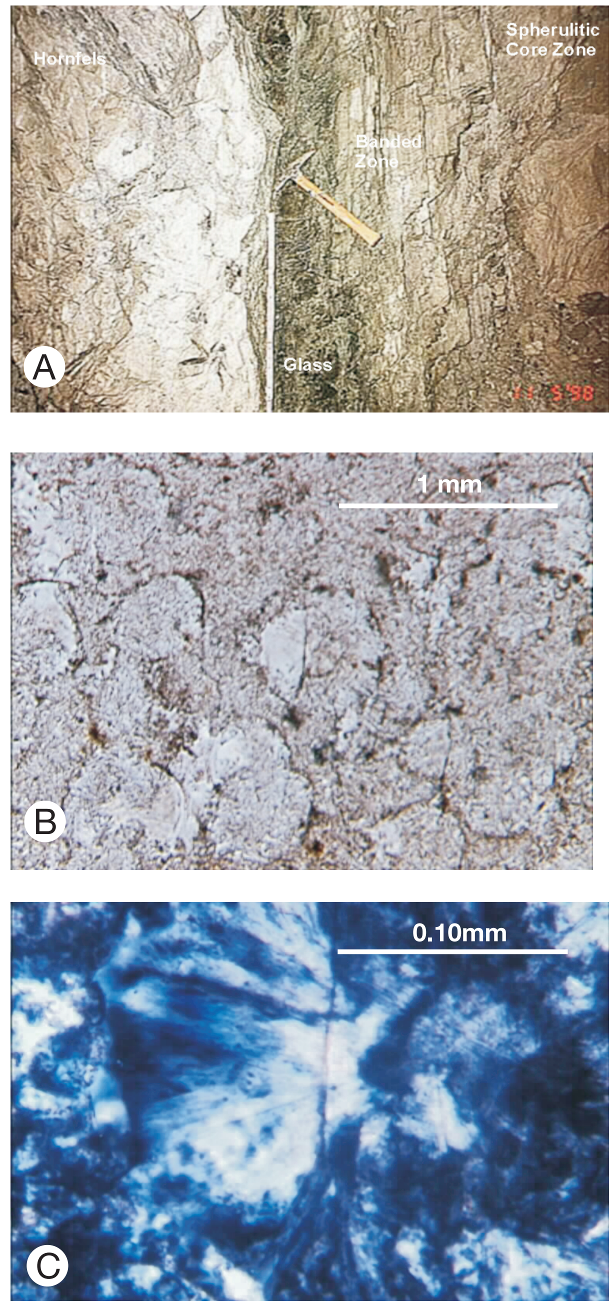

FIG. 6. Photograph and photomicrographs of Deep Star rhyolite from the Deep Star deposit, Nevada. A. Contact of Deep Star rhyolite (hammer head for scale) with calc-silicate (light-colored rock) and irregular green glass that gives way abruptly (mid-hammer handle) to flow-banded rhyolite. Far right-hand side of photograph consists of the spherulitic core zone of the exposure. B. Photomicrograph (plane-polarized light) of spherulitic Deep Star rhyolite with interstitial quartz and finely crystalline alteration products—primarily kaolinite. C. Photomicrograph (crossed nicols) of a single sanidine spherulite in a central core of a Deep Star rhyolite dike.

a banded interval of rhyolite is present between the glass and massive dike core (Fig. 6A). Rhyolite within the Deep Star orebody ranges from 0.25 to 12 m thick, has a fine-grained sugary texture, and is commonly pervasively altered. Within the orebody, glass has been altered to a green, waxy smectite whereas the spherulitic core is altered to quartz, nontronite, sericite, and marcasite.

At least two stages of Deep Star rhyolite emplacement occurred syn- or preore, and postore. The former is locally brecciated, weakly mineralized, and crosscut by the latter (Fig. 7). Texturally and mineralogically syn- and postore rhyolite dikes are strikingly similar and are interpreted to be part of the same igneous event; however, the older dike may be syn- or immediately preore but does not display evidence of having undergone the alteration of Jurassic dikes in the area. Field relations, with one dike wholly intruded into the other, indicate that both were intruded during a relatively short geologic time span, under similar tectonic conditions (i.e., stress states). The absence of reactivation at this contact, which is present on the outer margins of this fault, precludes a significant time hiatus between emplacement of the two dikes. In several localities, the postore dike contains argillized and mineralized calc-silicate fragments in its glassy margin. Ressel et al. (2000) reported an imprecise $^{40}Ar/^{39}Ar$ date of 38 Ma from the Deep Star rhyolite. Other dates from different locations in the deposit, but also within the postore dike, include 38.05 ± 0.09 Ma (T. B. Thompson, this report) and 38.98 ± 0.26 Ma (M. Ressel, unpubl. data, 2002). Reliable dating of the older synore rhyolite was not possible due to alteration.

The Deep Star rhyolite dike that intruded the Gen fault has a consistent 9 to 10 m thickness. Rhyolite in the Deep Star fault ranges in thickness from less than 1 m to 9–10 m and is more altered and sheared than the rhyolite in the Gen fault. Northeast- and northwest-striking rhyolite dikes and sills extend across the orebody. In the upper mine levels, a continuous northeast-striking body of rhyolite forms the northern boundary to the orebody and is known as the Northeast break (NEB). Synore dikes and sills are intimately associated with high-grade ore throughout the mine. The Anne dike, exposed in the Genesis open pit to the south, is compositionally similar to the Deep Star rhyolite.

Several highly altered dikes present in drill holes within the Deep Star and Post faults consist of green clay with unaltered, euhedral biotite phenocrysts. These are interpreted as biotite-feldspar porphyry (bfp) and may be related to the 40 Ma K dike exposed at Genesis (M. Farmer, written commun., 1995) and/or similar biotite-feldspar porphyry dikes at the Betze-Post deposit (Arehart, 1993a; Mortensen et al., 2000). Positive petrologic identification is difficult due to limited exposure and the highly altered nature of these dikes. A recent $^{40}Ar/^{39}Ar$ date on fresh biotite from one of these dikes within the Deep Star fault yielded an age of 39.67 ± 0.21 Ma (M. Ressel, unpubl. data, 2002). The relationship of the biotite-feldspar porphyry dikes to the gold mineralization is unknown, as they have only been identified peripheral to the deposit.

Structure

Structural observations and background

A complicated structural history, possibly beginning with Late Proterozoic rifting of the continental margin (Dickinson, 2001), produced a complex structural framework in the

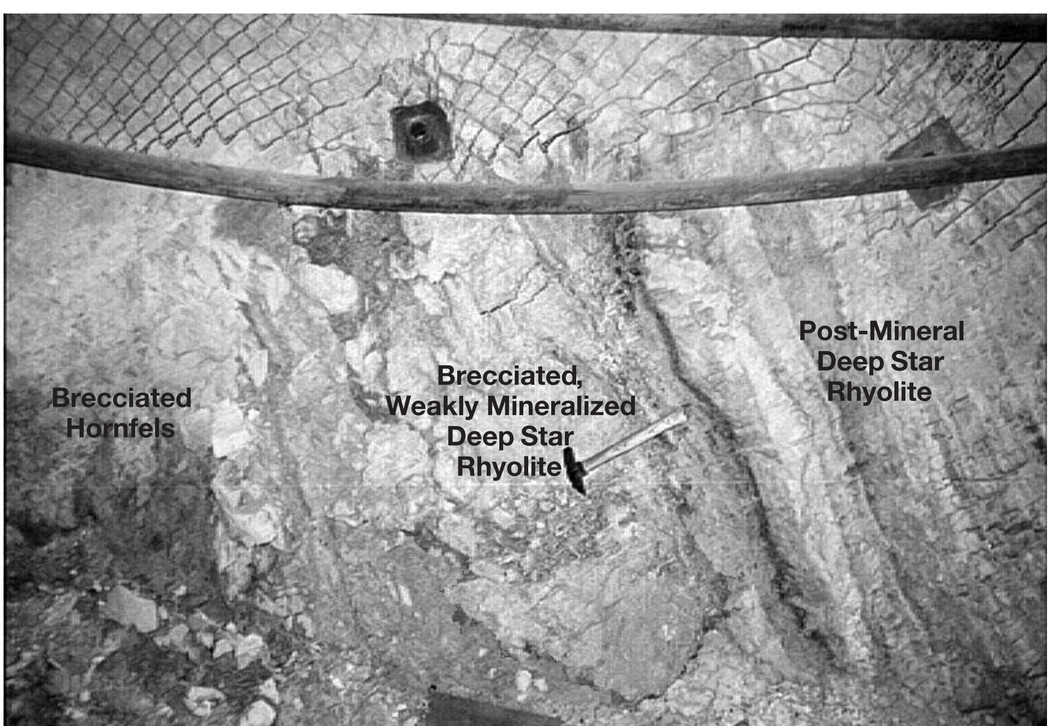

FIG. 7. Late ore-stage brecciated Deep Star rhyolite with sulfidic matrix cut by postore Deep Star rhyolite dike with glassy chill margin.

northern Carlin trend. This deformational sequence includes east-directed contractional deformation attributed to the Antler orogeny, pre-Late Jurassic separation on the Gen-Post fault system, Late Jurassic intrusion of the Goldstrike diorite, followed by east-northeast-directed shortening to form the Tuscarora anticline, Late Jurassic relaxation and intrusion of lamprophyre dikes on north- and northwest-striking faults and/or fractures, and two distinct episodes of Tertiary extensional deformation involving reactivation of existing structures and intrusion of late Eocene dikes along north- and northeast-striking faults and fractures. Other than synore and postore Eocene dikes (38 Ma), geologic elements that constrain the age of faulting (i.e., radiometrically dated or by demonstrable field relations) are the Late Jurassic Goldstrike intrusion and lamprophyre dikes (about 158 Ma) and the Miocene Carlin Formation (about 15 Ma; Fleck et al., 1998).

Most regional structures in the Carlin trend developed prior to gold mineralization. Simplistic or Andersonian (conjugate) structural models using plan map geometry are generally inapplicable (Fig. 2). The assumption of homogeneity within the host rocks, a requirement of such analysis, is invalid. Earlier structural elements appear to have influenced the formation of later ones. Faults with inhomogeneous crosscutting relationships, multiple sets of slip indicators, and stratigraphic separations that are inconsistent with slip indicators demonstrate that reactivation of earlier formed faults is common (P. Lewis, written commun., 2001).

Structural analysis

The major faults were studied with a focus on kinematics, and the results compared with the regional structural framework and known field relations at other deposits on the Carlin trend. These data were integrated with three-dimensional deposit modeling using drill hole and mining assay information. Linking three-dimensional deposit models on the basis of Newmont's database has allowed correlation of structural features over a 4-km strike interval along the Gen-Post fault zone from south of the Genesis deposit through the Betze-Post deposit.

The primary structural characteristics considered in this analysis include kinematic indicators on faults, crosscutting fault relationships, fault separations, fault geometry and continuity, fault-fracture filling (gouge, cataclasite, etc.), and proximity or relation to gold-mineralized rocks (Figs. 8 and 9). Kinematic indicators, such as slickenlines, mullions, gouge fabrics, and subsidiary structures (Riedel shears), were measured to determine the net slip axis and sense of slip for major faults and sets of faults. Over 80 slickenline measurements from north- and northwest-striking faults demonstrate a pronounced southerly rake indicating oblique slip (Fig. 10). Mullions, synthetic shear fabrics (R1 Riedel shears), and fault gouge fabrics, considered more reliable than slickenlines because they are not as easily overprinted and require substantive fault movement to form, corroborate oblique dextral-normal slip on north- and northwest-striking faults and oblique sinistral-normal slip on north-northeast- and northeast-striking structures. Care was taken to record overprinting sets of slickenlines, and two populations of slickenlines were consistently observed on many north- and northwest-striking fault surfaces.

Fault geometry

Deep Star is bounded on the west by the Gen fault and on the east by the Deep Star fault, lying within the Gen-Post fault system (Figs. 8 and 9), a major north-northwest-striking Mesozoic or older structure with over 12.5 km of known strike length (Fig. 2). The Gen-Post fault system has a complex structural history of reactivation, with the Deep Star fault as an internal strand between the Gen fault, which extends to the south, and the Post fault, which continues to the north. The north-striking Deep Star fault serves to accommodate a bend in the Gen-Post fault system where it intersects the Jurassic Goldstrike intrusion; the Gen and Post faults to the south and north, respectively, strike north-northwest (about 340°). Latest slip on the Gen-Post fault system cuts apophyses of the Goldstrike intrusion, but larger magnitude separations are evident in adjacent Paleozoic rocks, indicating that the fault existed pre-Late Jurassic. The fault zone is locally intruded by both Jurassic and Eocene dikes (Fig. 11). At the 4,600-ft mine level, the Gen, Deep Star, and Post faults are separated from one another by about 60 to 100 m horizontally, strike north-south, and dip eastward (60°–75°). At Deep Star, gouge fabrics and slickenlines indicate oblique dextral-normal slip on the Gen fault with a minimum of 60 m of apparent normal separation on the basis of stratigraphic relations. The Deep Star fault shows similar oblique dextral-normal slip with approximately 183 m of apparent normal separation of the Roberts Mountains thrust (Fig. 5). Two episodes of oblique dextral-normal slip are documented on the Deep Star fault, the earlier with a greater strike-slip component of displacement and the later with a greater dip-slip component (Dunbar, 2001). These displacements are likely the most recent and, on the basis of regional constraints, probably represent late Eocene and Miocene extension, respectively (Seedorff, 1991). Fracture density within the orebody is higher than in surrounding rocks and increases eastward toward the Deep Star fault, as does the intensity of brecciation and gold grade. Protracted faulting also is shown across the Gen fault by only 37 m of normal dip separation of the Miocene Carlin Formation gravels at south Genesis, as opposed to over 250 m for the Roberts Mountains thrust (Schutz and Williams, 1995).

Brittle faults and fractures are the most prevalent and dominant structural features in the mine, although minor folds in bedding can be observed in the upper levels and on the western margins of the deposit. All rocks at Deep Star, except the rhyolite and lamprophyre, have been folded at various scales; however, high fracture density, lack of detailed stratigraphic control, and brecciation precludes detailed fold analysis. On the mine scale, the north-northwest-trending Tuscarora anticline in the footwall of the Gen fault is subparallel to the strike of the Gen-Post fault system. Contoured poles to bedding recorded underground west of the Gen fault define a great circle girdle π-axis representing the anticline, whereas those recorded in the orebody east of the Gen fault exhibit a more diffuse, clustered pattern (Fig. 12A, B). Average bedding orientations differ across the fault, providing further evidence that the Gen fault represents a discrete structural domain boundary (i.e., the footwall of the Gen-Post fault system).

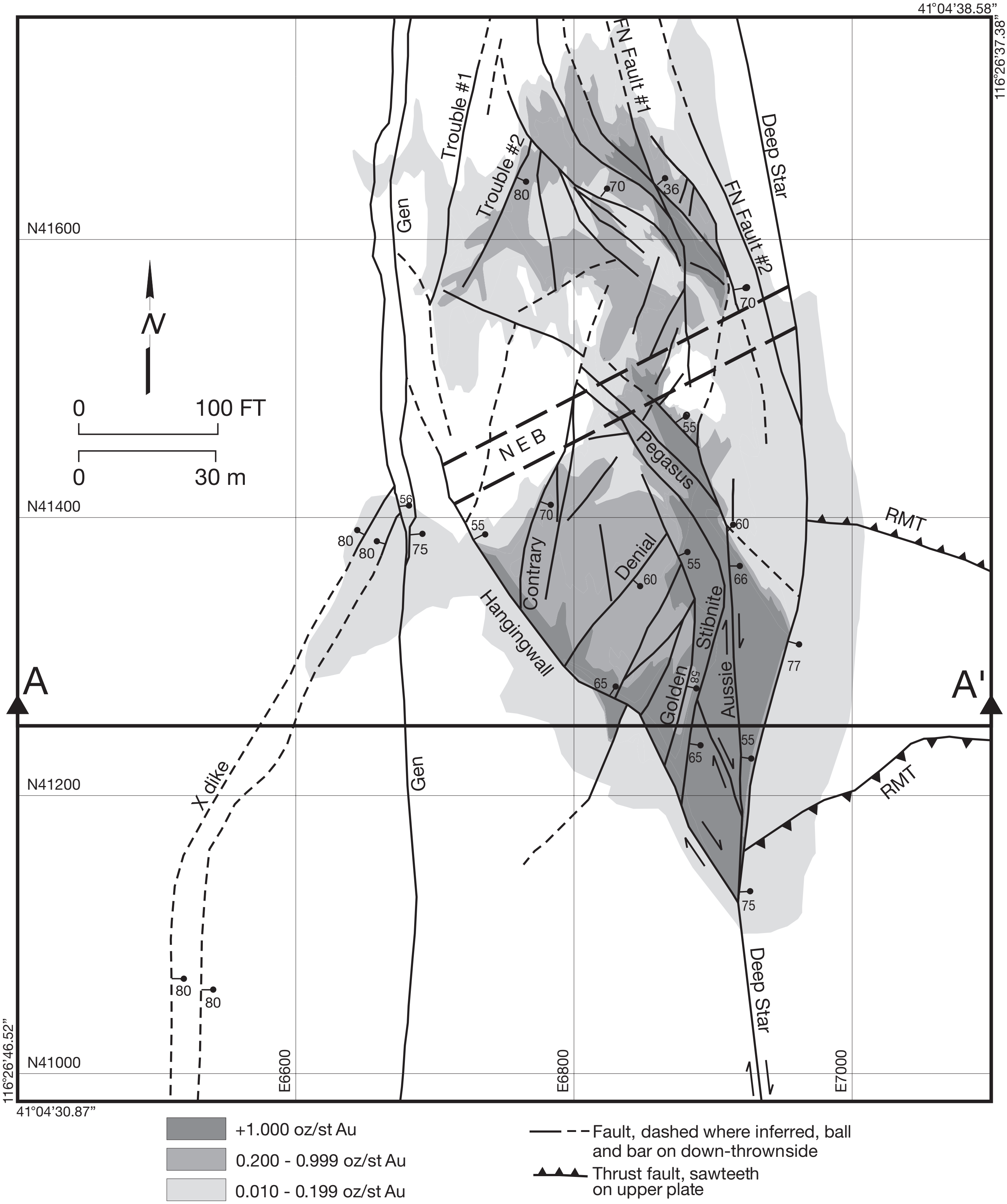

FIG. 8. Plan view of gold-grade contours at the 4570 A level, Deep Star deposit, Nevada. Gold contours represent a 3.5-m mining level and were drawn using gold assays from muck, rib, and diamond drill hole samples. A-A' shows the location of the N41250 gold contour cross section (Fig. 9). Local mine grid is in feet.

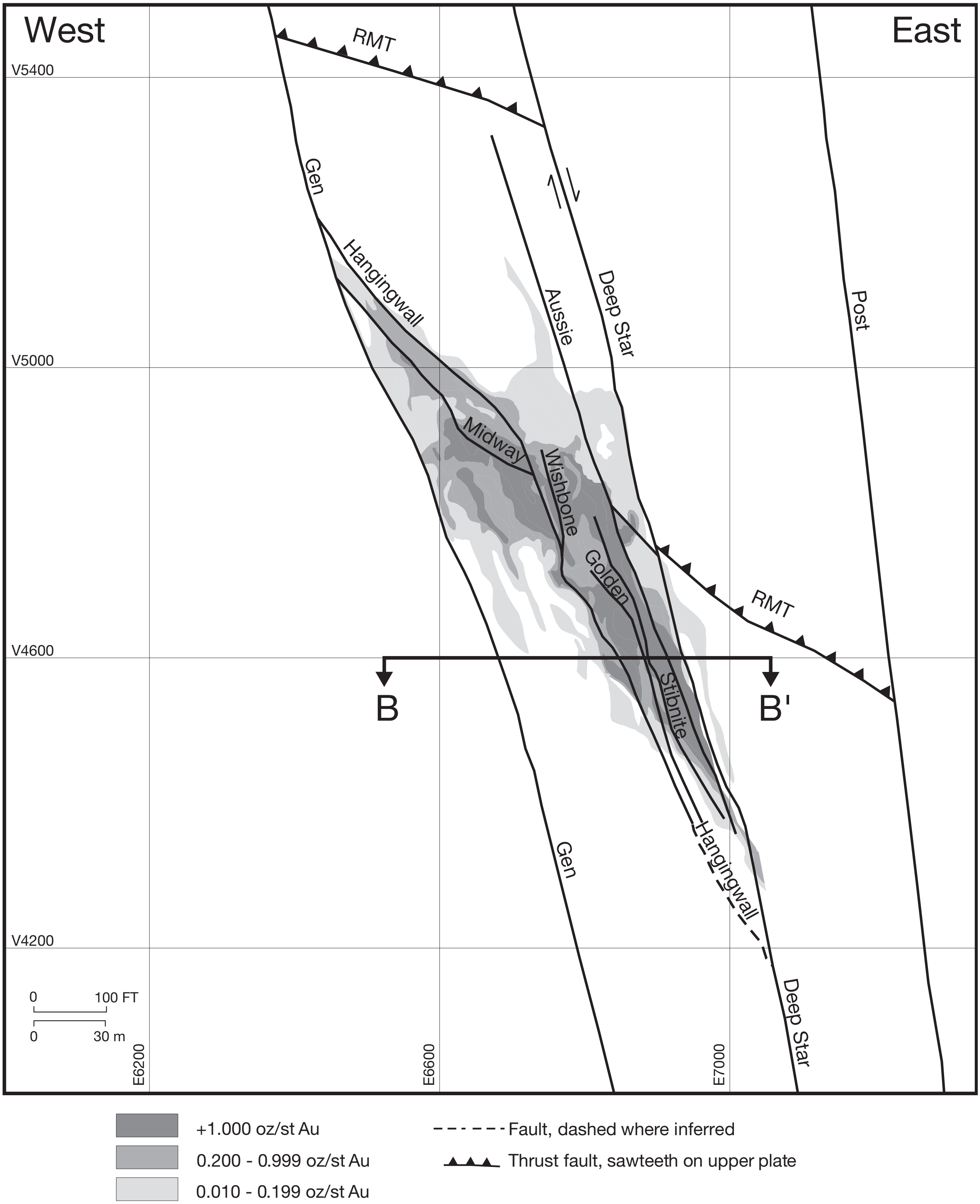

FIG. 9. Cross sectional view of gold grade contours on the N41250 section, Deep Star deposit, Nevada. Gold contours represent a 3.5-m mining level and were drawn using gold assays from muck, rib, and diamond drill hole samples. B-B' shows the location of the 4570 A level gold contour plan map (Fig. 8). Local mine grid is in feet.

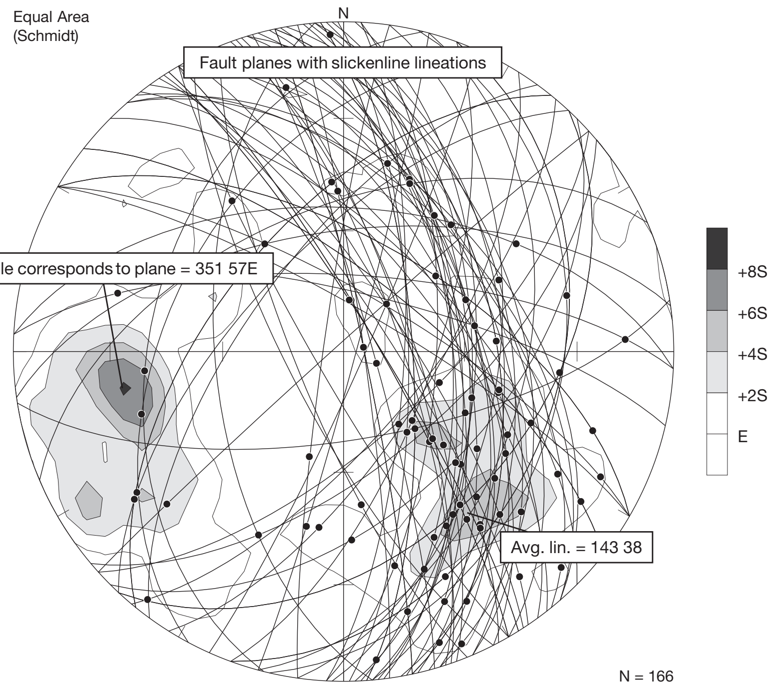

FIG. 10. Lower hemisphere equal area projection of fault planes at Deep Star, Nevada, each showing corresponding slickenline linear elements (n = 83). Contours to the left represent poles to fault planes (not shown), which average 351°/57° E in strike and dip; contours in the southeast quadrant are for slickenline lineations, of which the average plunge is 38° toward 143°. Avg. lin. = average lineation.

In the upper mine levels, the Gen fault (N 3° W/72° E) is the western limit to ore-grade gold, and the Hangingwall fault (N 42° W/64° E) is the eastern boundary. Progressing downward and eastward, ore grades are bounded by successive northwest-striking faults. On the 4,440-ft level, which is the lowest mining level, the orebody is only 3 to 15 m wide in the immediate footwall of the Deep Star fault but approximately 70 m east of the Gen fault (Fig. 9). The Hangingwall fault exerts a strong influence on present orebody geometry (Fig. 8). It is the hanging wall to ore in the upper levels of the mine (5,150–4,950 ft), cuts through the ore in the middle of the deposit (4,890–4,770 ft), and acts as the footwall in the lower levels (4,700–4,570ft). The Hangingwall fault clearly experienced postore separation and cuts all other faults except the Gen and Deep Star faults, into which it merges, creating the sigmoidal geometry observed on plan maps of Deep Star (Fig. 4). Three-dimensional structural reconstruction (unfaulting) of the 6.86-g/t modeled gold envelope across the Hangingwall fault (about 61 m normal-dextral slip) yields two parts which match up remarkably well, creating a stratiform shape similar to those of other Carlin-type deposits (Dunbar, 2001). The orebody was attenuated downdip to the east by postore separation along many faults that controlled synkinematic gold deposition.

The Deep Star fault was the primary local conduit for hydrothermal fluids during mineralization on the basis of grade distribution (Fig. 8), geologic mapping, petrography of alteration zoning, and geochemical modeling. The Deep Star fault is marked by a 12-m-wide clayey zone, containing several slip surfaces. A sinuous bend in the Deep Star fault, marked by a change in strike from north to north-northeast and back to north, is present between N41100 to N41400 (Fig. 8).

The Stibnite, Golden, and Aussie faults exhibit an arcuate geometry westward from their intersection with the Deep Star fault and the traverse brecciation which hosts ore-grade gold at Deep Star. These and lesser, unnamed faults coalesce in the lower, southern reaches of the deposit with the Hangingwall and Deep Star faults, and become subparallel to the Deep Star fault. Considered subsidiary structures to the Gen-Post fault system, these faults flare upward and westward away from this clay-rich zone of intensely fractured and sheared fault intersections, which represents the nucleus from which the highest gold grades decrease northward. The faults display a curvilinear, convex-east geometry in plan view, striking north or slightly north-northeast but trending more northwesterly away from the Deep Star fault toward the Northeast break dike (Fig. 4). Further, they exhibit the same slip sense and similar slickenline rake angles and gouge fabric orientations as the Deep Star fault. Jurassic diorite and lamprophyre dikes mapped on several levels at Deep Star occupy these structures, indicating their preore existence. The Aussie fault contains sheared carbonaceous material and essentially comprises the footwall of the Deep Star fault zone below the 4,640-ft level (Fig. 9). To the east between the Aussie and Deep Star faults, ore is hosted by a tectonic breccia.

In general, northwest-striking faults cut and displace northeast-striking structures and, like the Deep Star fault, show two populations of slip indicators within the ore-grade breccia, implying two episodes of postore movement (Fig. 8). Faults that strike more northwesterly, such as the Midway,

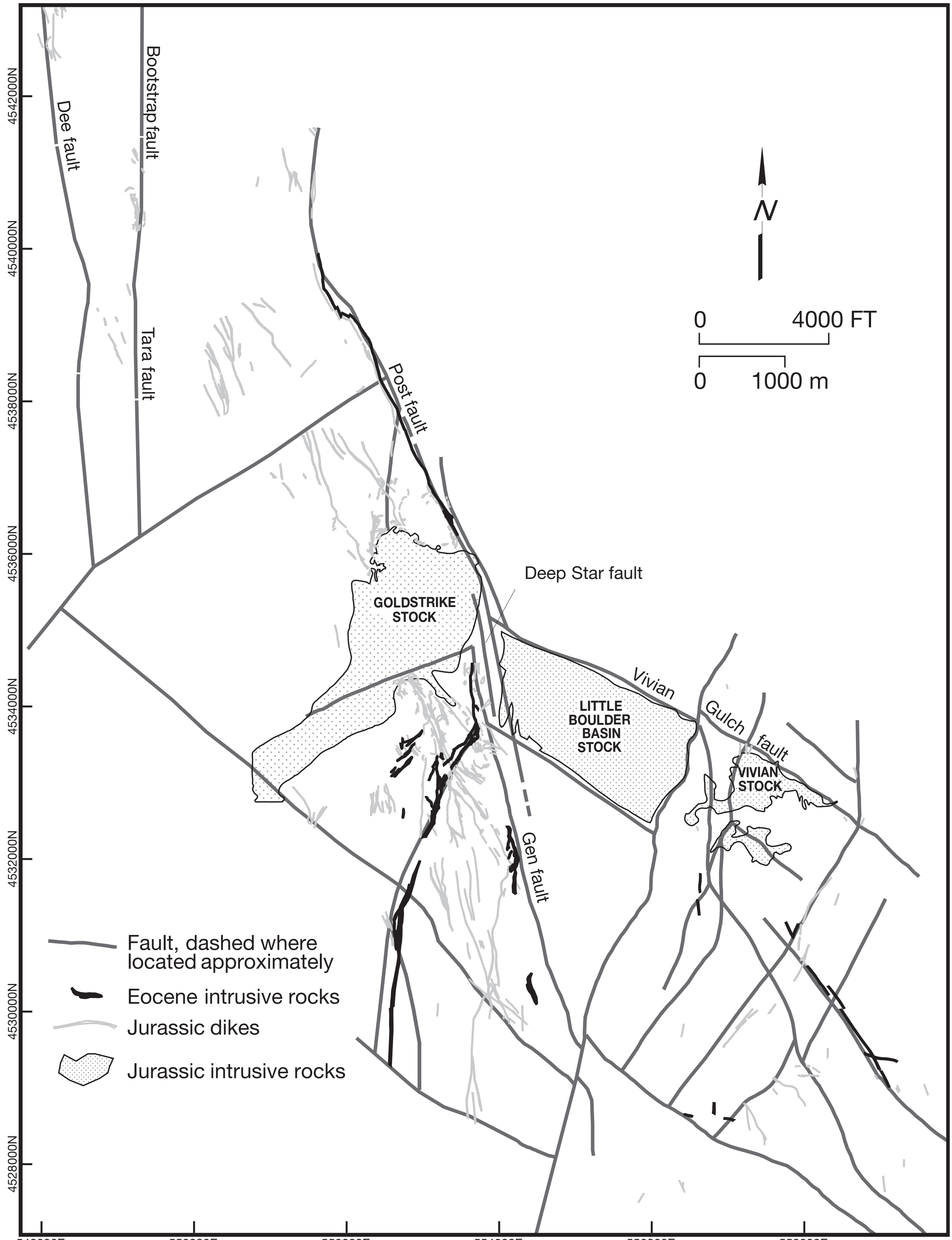

FIG. 11. Major faults and intrusions of the northern Carlin trend, Nevada. Northwest-striking Jurassic lamprophyre dike swarm extending both north and south of the Goldstrike stock contrasts with Eocene rhyolitic to dacitic dikes striking generally northeast. Eocene dikes not visible at this scale have also been identified in the Gen-Post fault system at the Meikle, Betze-Post, and Beast deposits (Ressel et al., 2000).

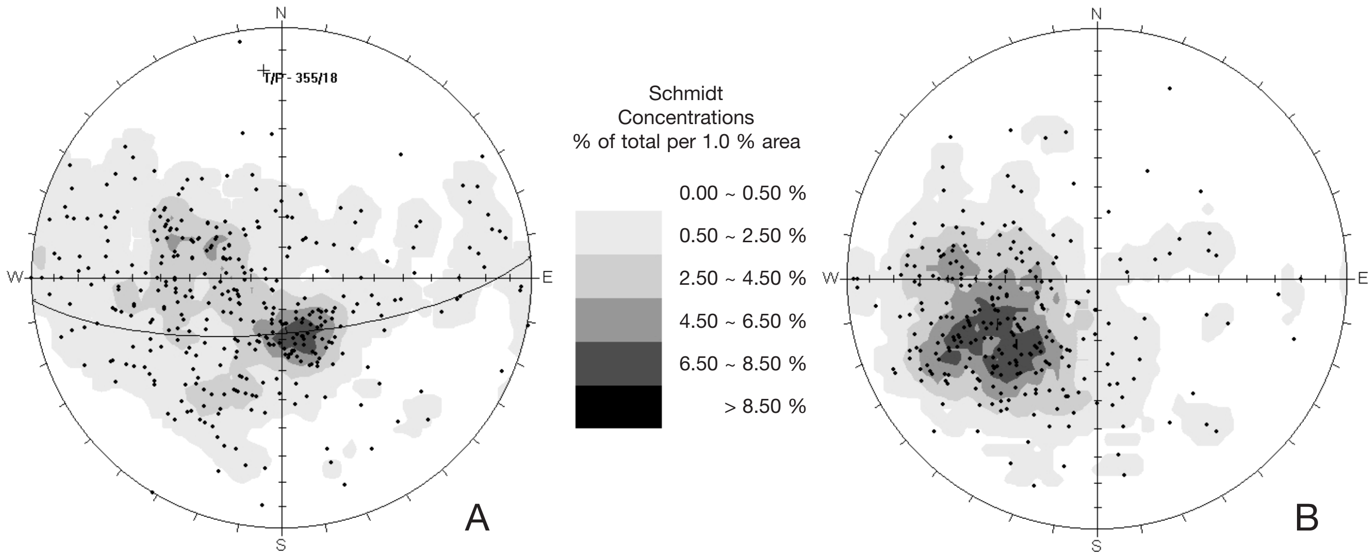

FIG. 12. Lower hemisphere equal area projections of contoured poles to bedding from the Deep Star deposit, Nevada. A. West of the Gen fault (n = 412), showing the π-axis with best-fit girdle representing the Tuscarora anticline, which plunges 18° toward 355° and the mean bedding plane strike and dip from contoured maxima of 254°/18° NW. B. East of the Gen fault (n = 280), primarily in the orebody, with mean bedding plane strike and dip of 329°/35° NE.

Wishbone, and Pegasus, subparallel to the Hangingwall fault, were not reactivated as recently and are usually cut by the north-northwest-striking faults.

Rhyolite dikes occupy portions of major structures, and numerous small apophyses are present in a number of unnamed faults that are mainly in the central part of the lower mine levels (Fig. 4). The Gen fault is occupied in places by two rhyolite dikes, one within the other, with both having chilled glassy margins. The dikes are otherwise compositionally very similar, suggesting that they were emplaced within a relatively narrow time span (Altamirano and Thompson, 1999; Ressel et al., 2000). Northwest-striking faults have dismembered a northeast-striking zone of rhyolites—the Northeast break—into discontinuous blocks, especially in the lower parts of the deposit. Thus, the Northeast break is a zone characterized by discontinuous northeast-striking rhyolite dikes, sills, and faults, which average N 65° E/48° NW and separate the main Deep Star orebody from the FN portion, north of mine grid N41430 (Fig. 8). Fault striae indicate sinistral normal slip (avg rake 24° SW), as do mullions along northeast-striking rhyolite contacts.

The FN-Royalty part of the orebody is characterized by shallow-dipping shear zones and faults subparallel to bedding planes. In general, this structural fabric dominates the geology of the north part of the mine, although a few widely spaced, steeply dipping faults show evidence of movement contemporaneous with these shallow structures. The shallow-dipping faults are continuous only on the scale of a few meters (as much as 15 m) and typically anastomose and splay into one another and/or the steeply dipping faults. Boudinage is clearly evident where individual beds can be traced. Gold-rich, sooty sulfide alteration (marcasite + pyrite) is concentrated along these shallow-dipping faults and preferentially mineralized bands and wedges (approx 0.2–1 m wide) associated with them.

Alteration and Mineral Paragenesis

Five general alteration assemblages, defined using X-ray diffraction (XRD) and petrographic studies of ore and waste samples, are used for underground mapping and core logging at Deep Star (Clode et al., 1997). Mineral assemblages are grouped for field identification and include propylitic, quartz-sericite-pyrite, quartz-dolomite, quartz-kaolinite, and argillic (Figs. 13 and 14).

T. Leach (written commun., 1999, 2000) and T.B. Thompson (this report) have studied the mineral paragenesis at Deep Star in detail. Both divided the paragenesis into similar alteration stages on the basis of petrography and XRD analyses. A combined paragenetic diagram is shown in Figure 15. "Argillic alteration" has been used in the field to describe clay minerals that were later determined to be associated with both stage 2 (propylitic–quartz-sericite-pyrite) and stage 4 (quartz-kaolinite) events. It is used most commonly to describe the altered rhyolite dikes but may be found in any rock type.

Stage 1 contact metamorphism and metasomatism is related to intrusion of the Goldstrike stock. Stage 2 includes quartz-sericite-pyrite and propylitic alteration, interpreted in this study as retrograde alteration associated with the cooling of the Goldstrike stock. Recent petrographic and XRD study shows that the sericite in the sedimentary rocks, originally grouped with quartz-dolomite (as quartz-sericite-dolomite; Clode et al., 1997), is in fact part of the quartz-sericite-pyrite assemblage present in the Goldstrike diorite and thus post-Late Jurassic in age. Stage 3 quartz-dolomite alteration is shown petrographically to postdate the quartz-sericite-pyrite event (principally the sericite) but is clearly preore. Stage 4 quartz-kaolinite alteration is related to the introduction of gold and is constrained in age by the postore Deep Star rhyolite. Argillic alteration typically includes intensely clay-altered (commonly smectite or kaolinite) diorite, calc-silicate,

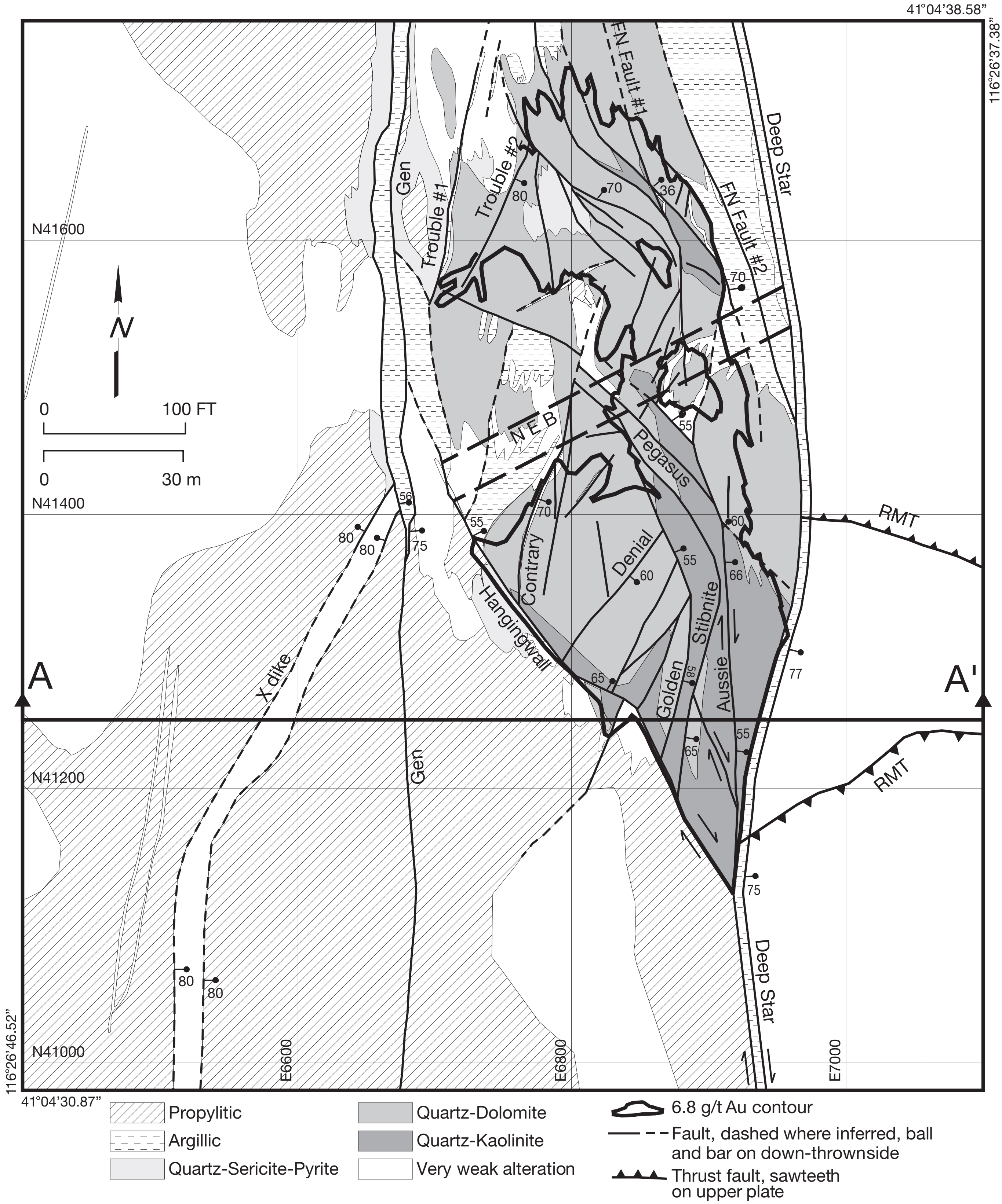

FIG. 13. Interpretive plan view showing mapped alteration zones on the 4570 A level at Deep Star, Nevada. The alteration was interpreted from underground mapping and core drilling. A-A' shows the location of the N41250 alteration cross section (Fig. 14). Local mine grid is in feet.

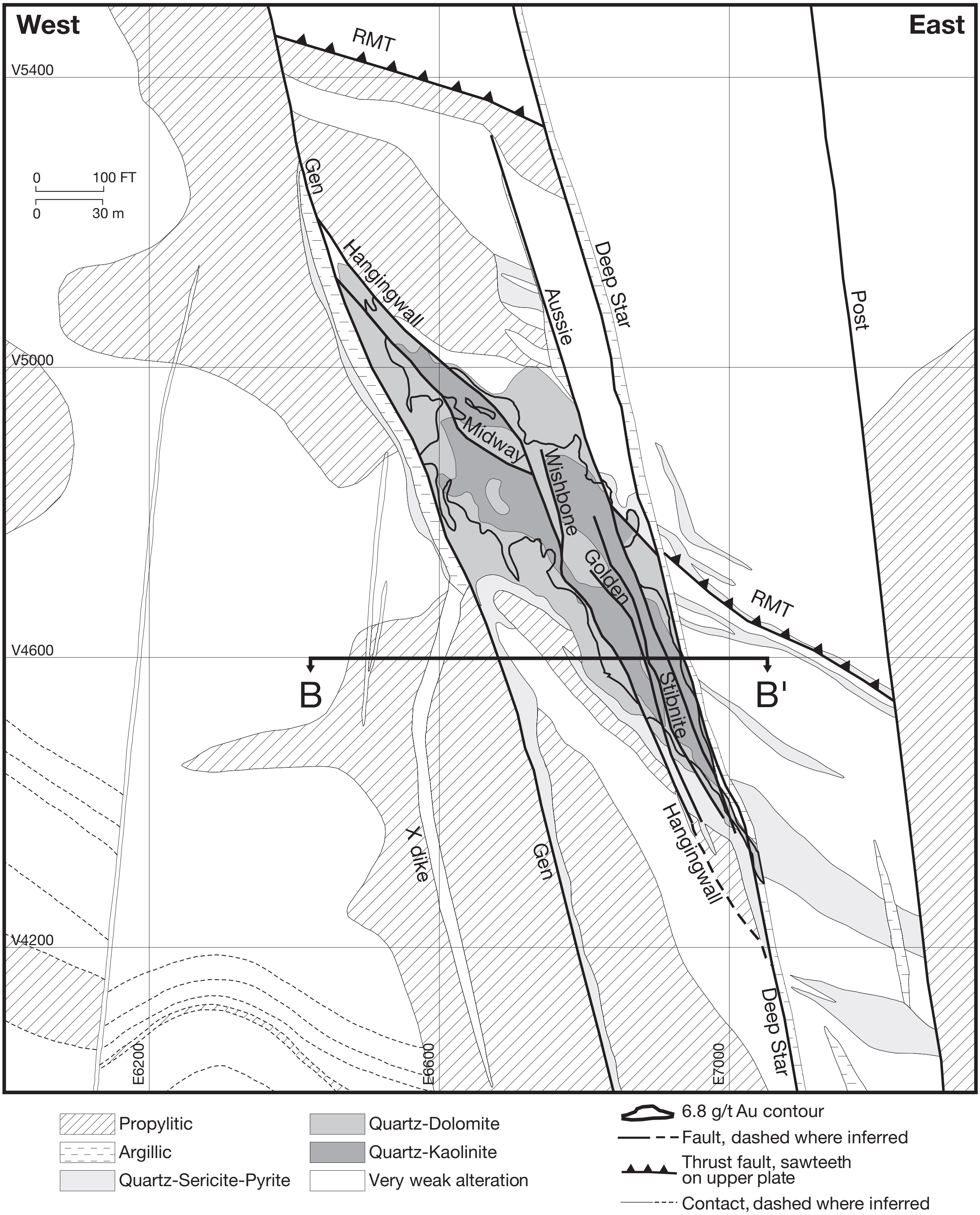

FIG. 14. Interpretive cross section showing mapped alteration zones on the N41250 section, at Deep Star, Nevada. The alteration was interpreted from underground mapping and core drilling. B-B' shows the location of the 4570 A level alteration plan map (Fig. 13). Local mine grid and elevations are in feet.

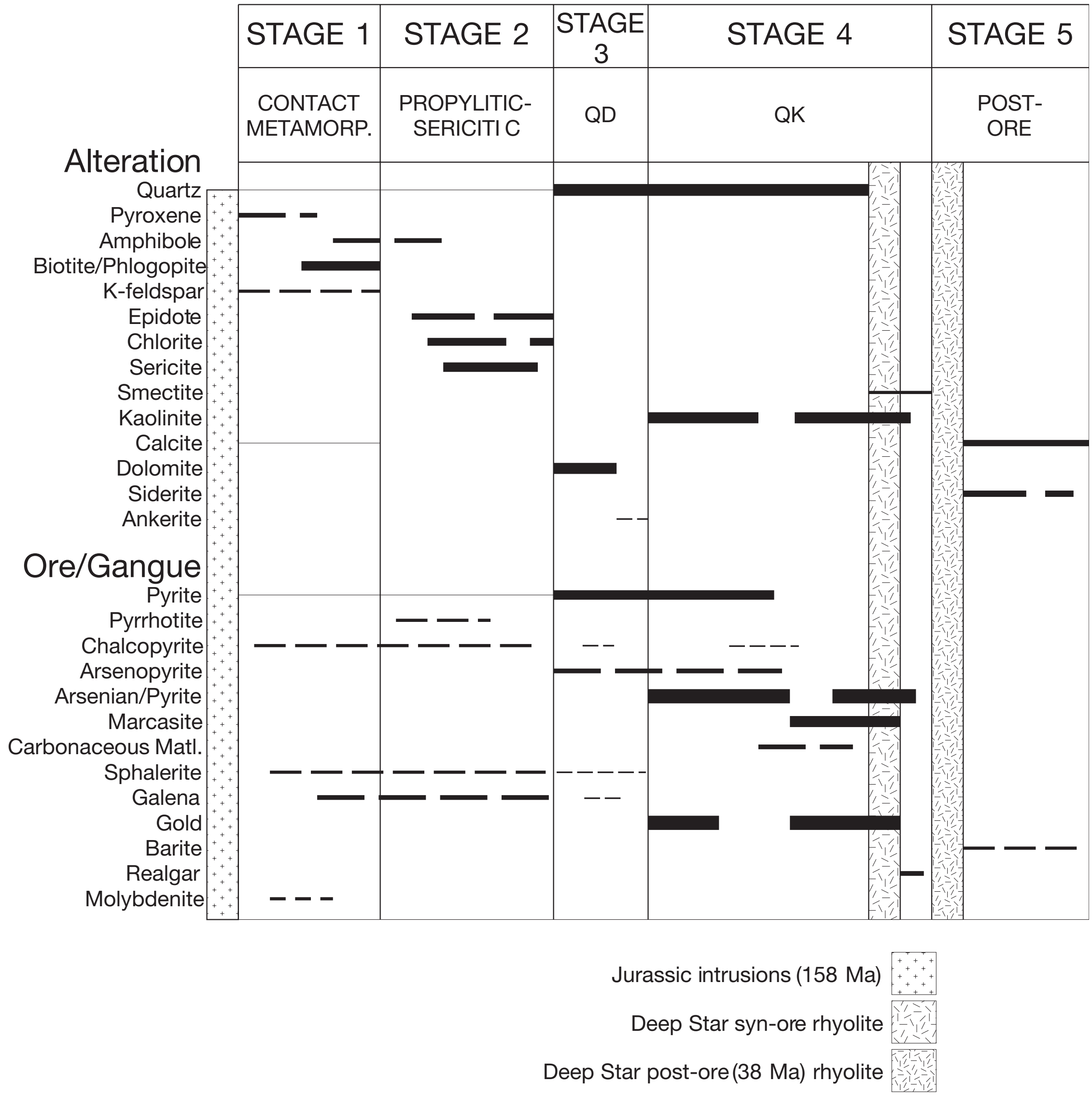

FIG. 15. Paragenetic diagram showing the stages of rock alteration at Deep Star, Nevada, with precipitation sequences for alteration assemblages and gold, sulfide, sulfate, and carbonate minerals relative to the Jurassic and Eocene intrusions. Line weights indicate the relative abundance of minerals. QD = quartz-dolomite alteration, QK = quartz-kaolinite alteration.

or Tertiary intrusive rocks occupying major fault zones or boundaries of the orebody, as distinguished from quartz-kaolinite alteration. Stage 5 is younger than the postore 38 Ma rhyolite, which is in turn unaffected by the mineralizing event.

Stage 1. Contact metamorphism and metasomatism: Lower plate, Paleozoic carbonate rocks in the area of Deep Star were altered to calc-silicate, phlogopite hornfels and minor marble or skarn assemblages. Upper plate siliciclastic rocks were altered to quartz hornfels, metaquartzite with lesser calc-silicate. The metamorphic aureole along the southern perimeter of the Goldstrike stock extends outward from the stock nearly 800 m. Silty carbonate strata were converted to finely crystalline quartz-diopside-calcite ± hedenbergite calc-silicate rock with locally abundant K feldspar, phlogopite, and biotite. Limestone was converted to diopside, grossularite, wollastonite, and calcite skarn or coarse-grained marble. Diopside-garnet endoskarn is present locally within the dioritic intrusions. Trace amounts of disseminated chalcopyrite, sphalerite, galena, and molybdenite are present locally in skarn. Quartz veins containing several percent euhedral molybdenite are present west of the Gen fault.

Stage 2. Propylitic–quartz-sericite-pyrite (QSP) alteration: Propylitic alteration of the granodioritic to dioritic Goldstrike intrusion is pervasive at Deep Star. Chlorite, epidote, calcite, sericite, and pyrite are present in most exposures of granodiorite, and largely replace biotite and hornblende, whereas plagioclase is selectively replaced by sericite. Chlorite and calcite dominate in propylitic zones and impart a medium- to dark-green color to Goldstrike intrusive rocks. Skarns also exhibit propylitic alteration. Trace amounts of sulfide minerals associated with this stage include pyrrhotite, chalcopyrite, sphalerite, and galena. Additionally, quartz-calcite veinlets crosscut the propylitized rocks. This assemblage is interpreted as the result of late-stage fluid interaction following the emplacement and cooling of the Goldstrike intrusive complex.

Sericite alteration effects on the diorite to granodiorite of the Goldstrike stock include local quartz-sericite-pyrite replacement of the rock. In hand samples, sericite is widespread and pervasive whereas quartz and pyrite are disseminated erratically in trace amounts. The timing of this event is poorly constrained but followed intrusion of the Goldstrike stock and preceded emplacement of the Deep Star rhyolite, as determined independently by both T. Leach (written commun., 1999) and T.B. Thompson (this study).

Quartz-sericite-pyrite altered diorite is generally pale yellow-green and is dominated by sericite with lesser quartz and pyrite. Weak quartz-sericite-pyrite alteration also is present locally in calc-silicate and skarn. Coarsely crystalline cubic pyrite in these rocks formed during diagenesis and following emplacement of the Goldstrike stock-sill complex.

Stage 3. Quartz-dolomite (QD): Quartz-dolomite alteration is preore and present in all rock types, except rhyolite, at the mine but is most strongly developed in calc-silicate rock. Associated minerals include 5 to 35 vol percent quartz, 15 to 50 vol percent dolomite ± ankerite, 0 to 20 vol percent calcite, and 0 to 15 vol percent sulfide minerals (pyrite and arsenopyrite), as determined petrographically by point counts. Quartz is present as finely crystalline replacements and discontinuous veinlets, whereas carbonate minerals are present as a matrix to other alteration minerals or in veinlets. Carbonate minerals are zoned from shallow levels on the west to deeper levels on the east and from northwest to southeast in the sequence: kutnahorite ⇒ ankerite ⇒ ankerite-dolomite ⇒ dolomite (T. Leach, written commun., 1999). Sulfide minerals are present as interstitial disseminations in finely crystalline (0.005–0.2 mm) aggregates, commonly with a dull brassy appearance. Sphalerite occurs in trace amounts associated with rare chalcopyrite and galena (T. Leach, written commun., 1999). In some veins (locally banded), stage 4 chalcedonic quartz is intergrown with the carbonate minerals, indicating a continuum of deposition from the quartz-dolomite to the quartz-kaolinite events (T. Leach, written commun., 1999).

Stage 4. Quartz-kaolinite (QK): Quartz-kaolinite and sulfide minerals are associated with the gold. Fine-grained quartz ± sulfide minerals and clays replace rocks affected by the stage 1, 2, and 3 events. Weak to moderate, pervasive to veinlet-controlled silicification is present locally and is typically observed outside of the +34-g/t Au zones. Fine-grained, pervasive silicification associated with barite and stibnite was intersected in drill holes along the Deep Star fault approximately 300 m below the deposit.

The quartz-kaolinite event includes a clay-rich, sulfide assemblage dominated by kaolinite and arsenian pyrite and marcasite (Fig. 16). On the basis of studies of other Carlin-type deposits, gold is hosted in arsenic-rich rims on marcasite and pyrite (Arehart et al., 1993b; Fleet and Mumin, 1997; Shallow, 1999). Clay minerals associated with the quartz-kaolinite event are zoned outward from a central core of intense kaolinite ⇒ weak-to-moderate kaolinite ⇒ smectite + kaolinite ⇒ illite (T. Leach, written commun., 1999). Smectite-dominated zones on the margins of the deposit are typically devoid of sulfide minerals and ore-grade gold.

Disseminated sulfide minerals associated with quartz-kaolinite alteration impart a dark, sooty appearance to the rock. Mineralogy of the sooty zones includes quartz, kaolinite, As pyrite, As marcasite, and relict arsenopyrite, chalcopyrite, and sphalerite from earlier stages. The fine-grained, sooty As pyrite + marcasite assemblage is distinctive and well constrained paragenetically relative to the preore coarse, brassy pyrite (Fig. 17A, B). Where pervasive, quartz-kaolinite alteration contains 5 to 20 vol percent kaolinite present in 1- to 2-mm bands and locally as "eyes" of green or blueish-green, coarse-grained kaolinite, 20 to 45 vol percent quartz as replacements and discontinuous veinlets, and 3 to 25 vol percent fine-grained sooty sulfide minerals (pyrite, arsenopyrite, and marcasite).

Locally, kaolinite is abundant in the older rhyolites, particularly adjacent to high-grade zones. Quartz-kaolinite alteration within rhyolite typically occurs on fractures with rare zones of replacement alteration containing gold grades of 3 to 6 g/t. Minor calcite is present, but none of the stage 3 carbonate minerals have been identified (T. Leach, written commun., 1999). The alteration paragenesis constrains the age of the older rhyolite as younger than the quartz-dolomite alteration and pre- or syn-quartz-kaolinite alteration.

Most of the Deep Star orebody is hosted in a breccia body that generally increases eastward in intensity from crackle, to clast-supported, to matrix-supported breccia (Fig. 18A–F). This gradation corresponds to increased intensity and pervasiveness of quartz-kaolinite alteration and higher gold grades. Breccias in the upper parts of the orebody are semiconformable with and grade into bedding (Fig. 18E). These breccias are truncated to the east by the Hangingwall fault. Clasts within this upper breccia body have their long axes locally aligned subparallel to bedding (Fig. 18F). Little rotation or transport of clasts is evident in the upper and western parts of the deposit, and fracture and/or fault density is less than below. Breccia distribution in the lower parts of the orebody, east of the Hangingwall fault, coincides with the north-northwest-striking, eastward dipping high-grade gold zone. Matrix-supported breccias, especially along hanging-wall faults (Hangingwall fault, Aussie fault, Deep Star fault, etc.), are typically broken and fractured, containing clayey, foliated fault gouge and tectonic breccia. This fault gouge and breccia was formed during postore faulting (Fig. 18D).

The matrix-supported breccias are typically multilithic. Breccia textures showing chemical dissolution and replacement of calc-silicate host rock by quartz-kaolinite-marcasite were described from petrographic and hand sample studies (Clode and McComb, 1993). T. Leach (written commun., 1999, 2000) also noted a progression from low gold grades in fractured rocks, through moderate grades in crackle and mosaic breccias, to high grades in matrix-supported fluidized breccias.

Clasts in the multilithic breccias are composed of quartz-dolomite altered calc-silicate, skarn, or diorite overprinted by quartz-kaolinite alteration as clast replacement, matrix, and veinlets. Subangular to subrounded clasts, which exhibit varying degrees of quartz-kaolinite replacement, can be identified in hand specimens, and fluid streaming textures are observed

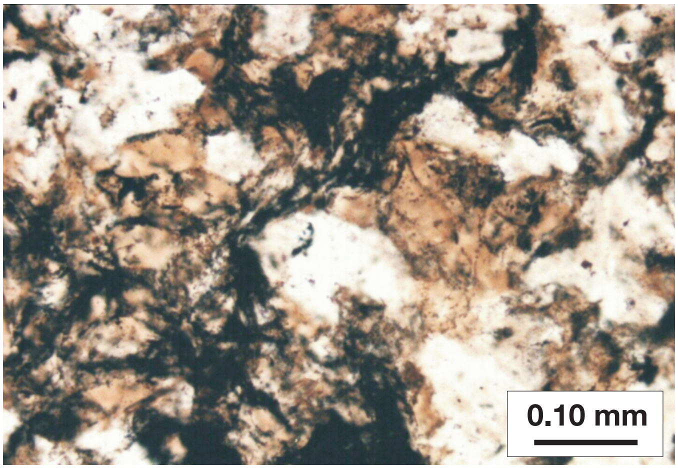

FIG. 16. Photomicrograph showing quartz (white)-kaolinite (light brown)-arsenian marcasite (black) within the Deep Star, Nevada, orebody. Note that kaolinite is intimately associated with marcasite.

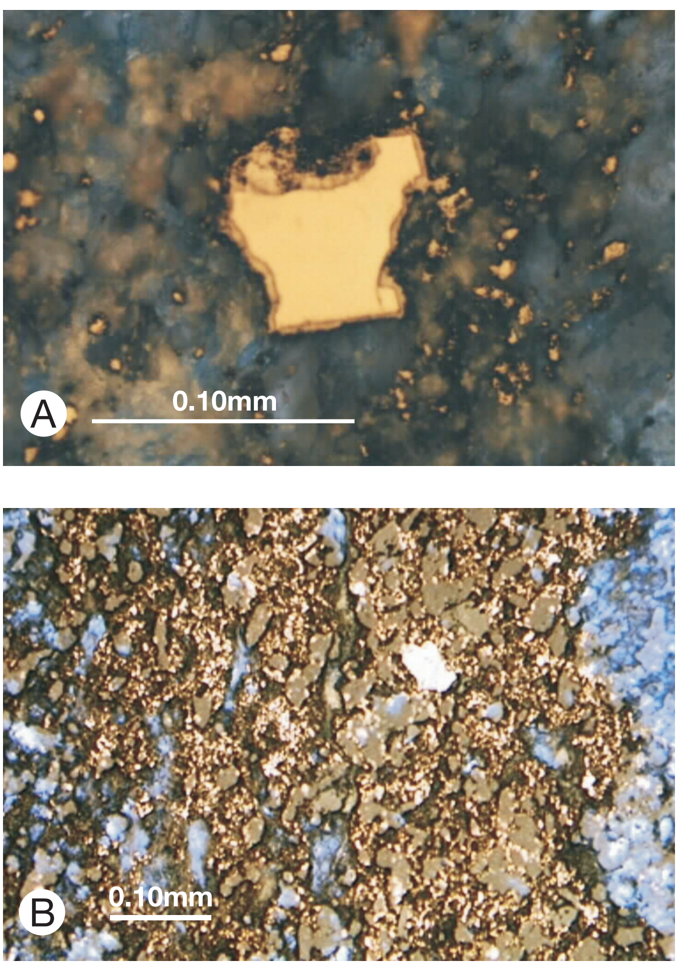

FIG. 17. Photomicrographs showing arsenian Fe sulfide minerals at Deep Star, Nevada. A. Large, early pyrite crystal with arsenian rim surrounded by finer, sooty arsenian marcasite in a quartz (light-colored) and minor kaolinite (dark) groundmass. B. Fine-grained, sooty arsenian pyrite and marcasite in quartz and kaolinite matrix.

locally within the matrix of intact brecciated rock. Breccia clasts are much smaller, more rounded, and sparse in the lower and eastern area. The quartz-kaolinite sulfide matrix progresses from microcrystalline veinlets in the quartz-dolomite crackle breccia in western exposures to 50 to 90 percent of overall rock volume in matrix-supported breccia to the east.

Increasing gold grades correlate directly with an increasing breccia matrix-to-clast ratio due to the greater abundance of fine-grained, gold-bearing sulfide minerals and clay in the matrix. Quartz-dolomite altered rock, more prevalent in the western portion of the deposit, is lower grade due to a reduced matrix-to-clast ratio. Higher gold grades are present where sooty sulfide minerals are concentrated. Moreover, the footwall of the Deep Star fault zone serves as a sharp boundary to gold grade in the lower levels of the mine (Fig. 8).

Realgar is distributed in discrete zones along the Hangingwall fault in the upper levels of the mine and southward where the Deep Star and Hangingwall faults merge in the lower levels of the mine. Realgar precipitated paragenetically late in stage 4 as veins, commonly containing euhedral crystals <3 mm long, and as distinct overgrowths on the ore breccias (Fig 15; Altamirano-Morales, 1999). Locally, realgar constitutes as much as 24 wt percent of the rock as determined by XRD. Carbonaceous material (remobilized pyrobitumen) is typically restricted to the Aussie fault and small irregular areas in its immediate vicinity.

The Deep Star rhyolite is intensely argillized close to the orebody where the rock is altered to nontronite, quartz, sericite, ± marcasite. Glassy margins of the rhyolite dikes are altered to a green smectite.

Fracture-controlled and poddy smectite alteration partly replaces calc-silicate and diorite wall rock on the margins of the deposit not bound by a discrete fault (e.g., south margin in the upper levels). Many ore-bounding structures, such as the Deep Star fault zone, contain intensely clay-altered diorite, calc-silicate rock, or Tertiary intrusions.

Stage 5: Calcite dominates the postore event and is commonly observed as euhedral crystals filling fractures and vugs. Minor clear quartz, clay minerals, barite, and siderite precede the latest calcite (Fig. 15). A zone of pervasive and fracture-controlled siderite, identified by XRD, was deposited as a 30- to 60-m-thick halo roughly 30 m above the orebody (P. Reichl, written commun., 1994). This siderite is interpreted to be related to the postore alteration; however, only minor petrographic work has been completed on this material due to a lack of exposure in drill core and underground workings.

Geochemistry

Sampling, analytical, and data display methodology

Newmont's onsite laboratory analyzed 1.5-m composited samples of drill core and cuttings for gold using a fire assay-atomic absorption method. Resulting pulps were composited to 6.1-m intervals and analyzed by commercial laboratories for trace elements by the following methods: GSI Laboratories (1990): Ag, Bi, Co, Cu, Fe, Mn, Mo, Ni, Pb, and Zn by aqua regia-organic extraction-atomic absorption spectrophotometry; As, Sb, and Tl by hydride generation-atomic absorption spectrophotometry; Hg by aqua regia-flameless atomic

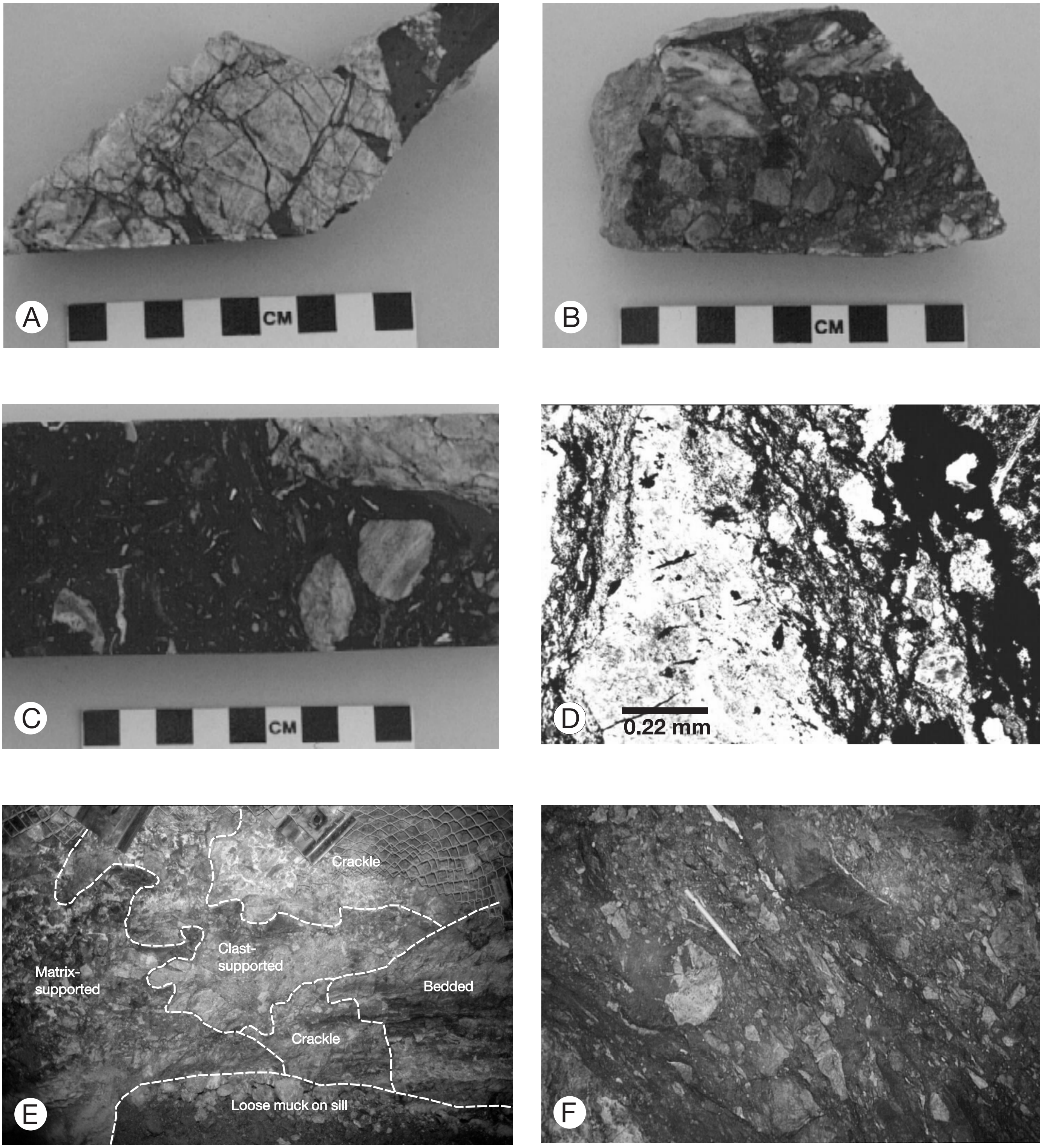

FIG. 18. Examples of breccias at Deep Star, Nevada. A. Representative sample of distal crackle breccia texture, showing large broken clast with gold-bearing, sooty sulfide veinlets. B. Intermediate clast-supported breccia with multilithic clast components. C. Matrix-supported breccia, showing increased volume of sooty sulfide minerals compared to A and B, and corresponding higher gold grade. D. Photomicrograph in plane-polarized light of silicified breccia with sooty and anhedral sulfide grains (black) in a quartz (white)-kaolinite(off-white) matrix. E. Gradation from weakly mineralized, bedded calc-silicate (right) to higher grade crackle and clast-supported breccia (left) (bolt plates are 0.3 m). F. Matrix-supported breccia; note distinctive alignment of clasts.

absorption spectrophotometry; and W by fusion-colorimetry, and Chemex Laboratories (1999-2001): Ag, Al, As, Ba, Be, Bi, Cd, Co, Cr, Cu, Fe, Ga, Ge, Hg, K, La, Mg, Mn, Mo, Na, Ni, P, Pb, Sb, Sc, Se, Sr, Te, Tl, Ti, W, U, V, and Zn by aqua regia-inductively coupled plasma-emission or mass spectrometry.

The bulk of the downhole data is of recent derivation. Older data were not used if shifts in relative accuracy compared to recent data could not be adequately addressed. A three-dimensional block model was created for each element after first log-transforming the data. Interpolated concentrations, at a grid node spacing of 30 × 30 × 12 m, were derived using an inverse distance squared algorithm and a 150 × 150 × 40-m search radius. The block models were displayed in three-dimensional space, using GoCAD software, along with fault and lithologic surfaces imported from the mine-planning three-dimensional models.

Geochemical overview

The geochemistry of the Deep Star deposit and the greater region of the Carlin trend is the product of several mineralizing events superimposed on the original bulk composition of the sedimentary and igneous rocks of the area (Kuehn and Rose, 1992; Hofstra and Cline, 2000). Mineralizing events identified in the northern part of the Carlin trend include a possible Devonian sedimentary exhalative origin for a portion of the gold and base metal sulfide minerals within the Popovich and Roberts Mountains Formations in the area of the Rodeo and Meikle deposits (Fig. 1; Emsbo et al., 1999). Emsbo et al. (2000) report Jurassic-age gold mineralization associated with quartz-base metal sulfide veins and widespread quartz-sericite-pyrite alteration at the Goldstrike deposit. Similar base metal mineralization associated with Jurassic-age stage 1 and 2 alteration events, but without gold, also was identified at Deep Star (Fig. 15). Alteration associated with emplacement of the Cretaceous Richmond stock (located approx 12 km southeast), and most importantly, with the Eocene intrusions also may have affected the geochemical patterns identified at Deep Star. Despite these previous effects, certain trace element zonation relationships relative to the orebody are evident in the vicinity of the Deep Star deposit.

In order to establish these zonation relationships, background concentrations of elements were estimated for the Popovich Formation, Vinini Formation, and Jurassic intrusions on the basis of "least altered" equivalents and these were compared to element enrichments in the Deep Star deposit and its vicinity (Table 1). In addition to gold, the deposit is enriched in As, Sb, Hg, and Tl by two orders of magnitude relative to background, similar to most Carlin-type deposits. This association is also consistent with the analyzed compositions of ore-stage pyrite and arsenian pyrite rim overgrowths on preore pyrite in other Carlin-type deposits (Fleet and Mumin, 1997; Simon et al., 1999; Cline, 2001).

The age of gold deposition in the Deep Star deposit is interpreted as Eocene on the basis of mineral paragenetic relationships and the age of altered intrusive dikes. Most rocks in the region have a strong overprint of the Eocene system as shown by the regional distribution of As, Sb, and Hg on the Carlin trend. For example, a comparison of the As content of Vinini Formation black cherts southeast of Deep Star to that of published data from the Tuscarora Mountains (Emsbo, 1993; Theodore et al., 2000) indicates an overprint of at least an order of magnitude. Similarly, the enrichment of these elements in the vicinity of the Deep Star deposit significantly

TABLE 1. Element Enrichment in the Deep Star Deposit Relative to the Upper Limit of Background in Host Rock Types

Element	Popovich[1,5] limestone (locally)	Jurassic[1,5] diorite (locally)	Vinini[1,5] chert (locally)	Vinini[1,2] chert (published data)	Deep Star[3,6] deposit	Deep Star[4,6] vicinity
Ag (ppm)	0.25	1	1	1.13	13	50
As	100	100	1,000	47	205,000	17,800
Au	035	035	035	038	90	3.500
Ba	650	650	650	n.d.	29,000	32,000
Bi	0.15	0.15	3	0.25	32	80
Cu	50	50	200	160	1,050	3600
Fe	25,000	55,000	40,000	30,000	150,000	150,000
Hg	1	1	1	0.80	645	30
Mn	400	1,000	1,000	6,000	2,700	>10,000
Mo	5	5	10	20	110	800
Ni	45	25	80	50	455	1,000
Pb	35	35	40	30	275	7,000
Sb	5	5	10	5	>10,000	3,000
Se	1	0.5	5	3	19	65
Te	05	05	0.30	0.30	84	19
Tl	1	1	2	0.25	600	20
U	5	3	6	n.d.	68	110
W	1	1	5	n.d.	275	400
Zn	200	200	350	120	>10,000	27,300

n.d. = not determined
[1] Upper limit of background range in least altered samples
[2] Emsbo (1993) and Theodore et al. (2000)
[3] Upper limit of values in Deep Star deposit
[4] Upper limit of values within 300 m of deposit
[5] Estimates for local background based on a drill hole database of 24,000 samples from the northern Carlin trend
[6] Estimates for the Deep Star deposit and its vicinity based on a drill hole database of 5,076 samples used in the 3-D block model

exceeds the background composition of the Goldstrike intrusion and Popovich Formation.

Many elements exhibit a closer spatial relationship to ore than to other geologic features, such as lithology or structure. These relationships were recognized by comparing the distribution patterns of trace and major elements to that of gold in three-dimensional space using GoCAD software. The following elements are interpreted to have been introduced or redistributed by hydrothermal fluids in the vicinity of the Deep Star deposit: Ag, As, Au, Ba, Bi, Ca, Cd, Co, Cu, Fe, Hg, Mg, Mo, Mn, Ni, P, Pb, S, Sb, Se, Te, Tl, U, V, W, and Zn (Table 1 and Fig. 19). The three-dimensional distribution patterns of these elements define a vertical plume that crosscuts stratigraphy and flares out to the west above the deposit. At elevations below the deposit, the plume is focused between the immediate footwall of the Deep Star fault and the Post fault. At the level of the deposit, the plume encompasses both the Deep Star-Post fault corridor and the Deep Star deposit in the footwall of the Deep Star fault. Above the deposit, it is broadly dispersed laterally as well as vertically.

Element zonation

The vertical plume described above is zoned laterally in relation to the position of the Deep Star deposit as reflected in a number of different element associations: (1) Au, As, Hg, Sb, Tl, W, ±Ag, Zn enrichment; (2) Ca, Mg, Ba, Sr depletion; (3) Fe, Mn, Co, Ni, P enrichment; and (4) Pb, Bi, Cu, Mo, U, V enrichment. The interrelationship of these zoned associations is best expressed on cross section N41375 using representative elements from each group (Fig. 19).

The distribution of high-grade gold (>3.5 g/t) is restricted to the Deep Star deposit; however, an area of anomalous gold (>0.1 g/t) is evident above and below the deposit (Figs. 19 and 20). This zone of anomalous gold concentration indicates a vertical plume with its roots developed below the level of the deposit and positioned toward the south end and east of the Deep Star deposit between the Deep Star and Post faults. The gold plume exits above the deposit, toward its north end in the footwall of the Deep Star fault, and flares out toward the west. Overall, the trend of the plume is from east-southeast to west-northwest and roughly approximates the strike of the Hangingwall and Pegasus faults within the orebody.

The upper portion of the gold plume, 300 m above the deposit, is hosted in the Goldstrike intrusion as a horizontal blanket immediately above the redox boundary. This blanket extends northward toward the Deep Post deposit and is host to several small near-surface oxide deposits (i.e., Pancana). The pattern suggests that supergene weathering processes have mobilized gold present in the exit plume and redeposited it in the oxide zone just above the redox boundary. Such supergene weathering effects have been documented in other parts of the Carlin trend, most notably in the Mike deposit beneath Carlin Formation of mid-Miocene age (Norby and Orobona, 2002). Additional evidence for a supergene origin for this feature is the general absence of As, Sb, and Hg associated with the gold enrichment. These elements invariably show a strong increase and correlation with gold in hypogene ores but display significantly weaker correlation coefficients in oxidized ores.

The Deep Star deposit is enriched in As, Sb, Hg, Tl, and W, with a weaker association of Zn and Ag. Of these elements, Hg is the most strongly correlated with gold on a bulk sample basis. Many trace element studies, using SIMS analyses of ore-stage arsenian pyrites, have emphasized the close association of gold with As (Arehart et al., 1993a; Fleet and Mumin, 1997; Simon et al., 1999; Cline, 2001); however, on a bulk sample basis, this close association breaks down because of the overprint of late-stage realgar and orpiment deposited as open-space fillings. Silver and Zn, although anomalous in the deposit, are more strongly anomalous east of the deposit between the Deep Star and Post faults within the feeder zone (Fig. 19). The distributions of Zn and Ag, both on section N41375 (Fig. 19) and in three dimension, closely resemble those of Au, As, Sb, and Hg, although some differences are observed above the deposit. A preferential increase along the Roberts Mountains thrust also is observed for As, Hg, and Zn. The association of Zn with deposits on the Carlin trend is common (Deep Post, West Leeville, Carlin Underground, Rain, Gold Quarry, Mike) although not well documented in the literature. This may reflect the selective characterization of ore samples in deposit studies and the lack of wider ranging data that would otherwise reveal a spatial association of gold with base metals. Like Au, the elements Zn, Ag, and W may not be present in sufficient quantity to form separate mineral species but rather may be present in solid solution within ore-stage pyrite as observed in the Getchell deposit (Cline, 2001).

Roughly coincident with the location of the anomalous Au, As, Sb, and Hg are low concentrations of aqua regia-extractable Ca, Mg, Ba, and Sr. This signature is strongest in the Popovich Formation between the Gen and Post faults, but it extends up into the Vinini Formation to elevations at least 180 m above the top of the deposit. Aqua regia is an effective digestion for carbonate minerals but not for alumino-silicate or sulfate minerals. Therefore the distributions of Ca, Mg, Ba, and Sr are interpreted to reflect the extent of decarbonatization in the vicinity of Deep Star. Decarbonatization extended into the footwall of the Deep Star fault resulting at least in part in the formation of collapse breccia. This is supported by visual observations of decarbonatization textures on both sides of the fault. This same volume of rock is enriched in Au, As, Sb, Hg, and base metals, suggesting that ascending mineralizing fluids followed this zone of enhanced permeability.

The elements Fe, Mn, Co, Ni, and P show an increase in the immediate hanging wall of the Deep Star fault in the Popovich Formation and above the deposit locally within the Vinini Formation. The distributions of these elements do not appear to reflect the syngenetic composition of the host units since these patterns clearly crosscut stratigraphy and exhibit a strong spatial relationship to the Deep Star orebody. Also, areas of large amounts of Fe and Mn coincide with the location of stage 3—preore carbonate alteration (ankerite, kutnahorite, Mn-bearing dolomite) and stage 5—postore open-space-filling carbonate minerals (siderite, calcite). The distributions of Ni, Co, and P are similar to those of Fe and Mn, although the mineralogy of these elements is less certain.

Other elements that display vertical plumelike signatures include Pb, Bi, Cu, Mo, U, and V. Lead and Bi are anomalous

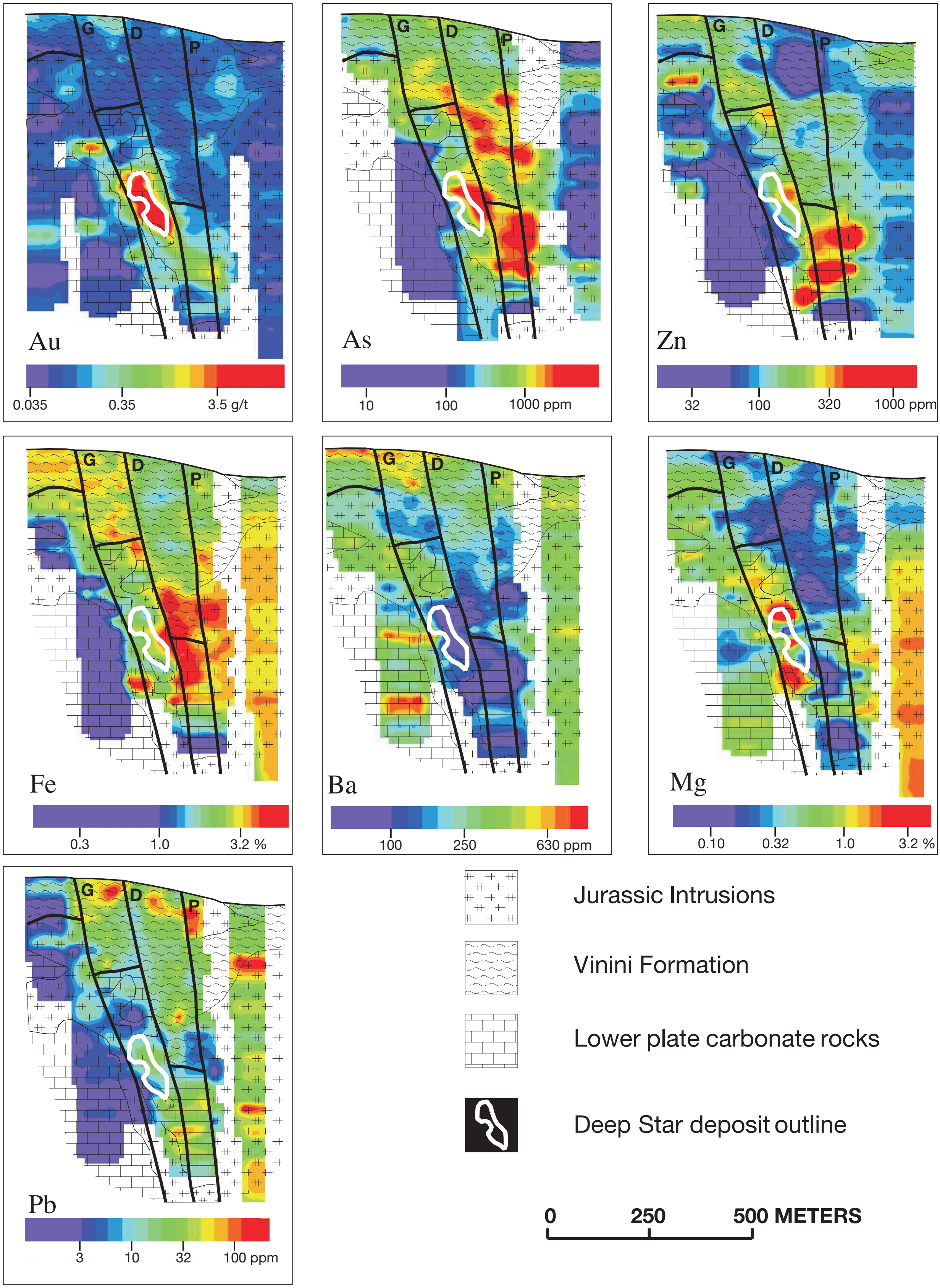

FIG. 19. East-west geochemical cross sections at N41375 through the Deep Star orebody, Nevada, looking north. D = Deep Star fault, G = Gen fault, P = Post fault.

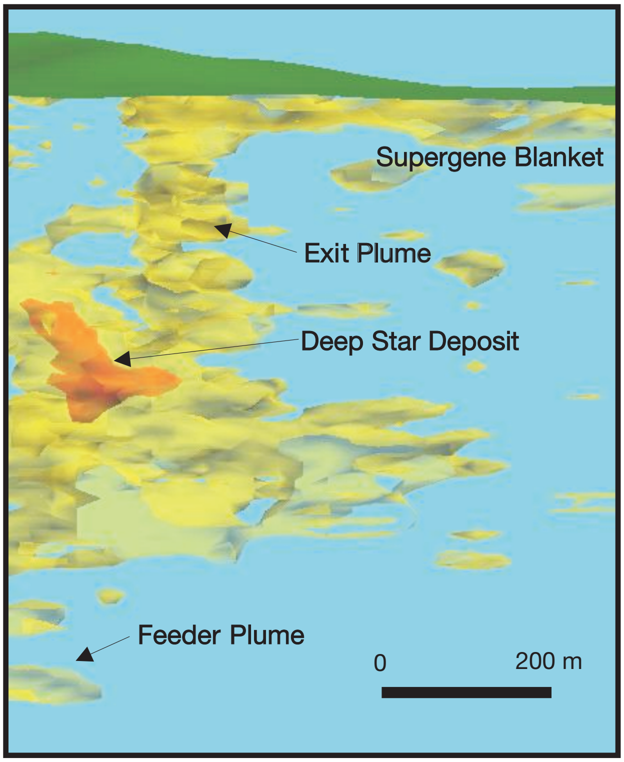

FIG. 20. Gold geochemical plume at Deep Star, Nevada. View looking west in a three-dimensional GoCAD model. Deposit shape is defined by a 3.4 g/t Au inner-grade shell. Plume is defined by a 1.4-g/t Au outer-grade shell. Dark surface at top of figure is the topographic surface.

in the Little Boulder Basin stock, east of the Post fault; however, these anomalies extend vertically into the Vinini Formation overlying the stock and westward into the footwall of the Deep Star fault. As reflected in surface sample data and the three-dimensional model, the Goldstrike and Little Boulder Basin intrusive rocks are generally low in base metals and have no base metal halos marginal to them. On the other hand, Pb and Bi are anomalous marginal to the Deep Star deposit, both in the stock and the feeder zone. The distribution patterns exhibit a plumelike geometry that crosscuts lithologic units and parallels other element patterns that appear to be related to the formation of the Deep Star orebody (i.e., Au, As, Hg). Similarly, Cu, Mo, U, and V distributions have a plumelike geometry. Collectively, these elements appear to be zoned laterally from east to west toward the deposit (Pb-Bi ⇒ Cu ⇒ Mo-U). The significance of this zonation is not known and the minerals hosting these elements have not been established.

The origin of elements which enrich the Carlin systems is controversial and it is difficult to separate, quantitatively, the contributions of the various mineralizing events that produce alteration overprints and geochemical increases and depletions. This is certainly the case for the Deep Star deposit; however, this study provides some constraints. Paragenetic relationships between ore-stage gold-bearing arsenian pyrite and the emplacement of rhyolite dikes provides a minimum age for the major pulse of gold mineralization as Eocene. The close association of anomalously increased or depleted elements with the distribution of gold and the appearance of systematic, though asymmetric, zonation in both trace elements and alteration mineralogy indicate that many elements were either introduced or redistributed by ore fluids originating from some depth during Eocene time.

It is possible that several mineralizing events separated by many millions of years could have followed the same fluid pathways and produced the same results. For example, decarbonatization leading to increased permeability could be related to a much earlier event than the one that deposited gold. The zonation relationships observed for the Deep Star deposit and other deposits on the Carlin trend, however, strongly suggest that most of the trace element patterns evident today are the result of a powerful mineralizing event which deposited gold in great quantities during late Eocene time.

Stable Isotopes

Twelve samples, containing significant kaolinite, were collected from the uppermost to lowermost levels of the mine workings (Table 2). The samples are representative of high-grade gold ore from the quartz-kaolinite altered zones on various mine levels (Fig. 14) and represent a vertical slice through the deposit. Separates were prepared by drilling individual kaolinite nests, veinlets, or flooded quartz-kaolinite material, followed by gravity separation. Some quartz contamination as determined by XRD was invariably present in the material analyzed. The kaolinite is intergrown with arsenian marcasite; no sulfide minerals, however, were present in the samples analyzed. Gold contents of most samples are indicated in Table 2, and those without analyses came from within the orebody. Figure 17B illustrates the intimate association of arsenian marcasite, quartz, and kaolinite. No sericite was detected under the microscope or by XRD analyses of the separates. Kaolinite δD and $\delta^{18}O$ data are presented in Table 2 and Figure 21.

Oxygen for stable isotope analysis was extracted from kaolinite separates by conventional fluorination techniques using BrF_5 as the reactant (Clayton and Mayeda, 1963). Mass spectrometric measurements were done on a Micromass Prism dual-inlet stable isotope ratio mass spectrometer.

TABLE 2. Kaolinite $\delta^{18}O$(‰) and δD(‰) Data, Deep Star Deposit, Nevada

Sample no.[1]	Mineral assemblage	$\delta^{18}O$ (‰)	δD (‰)	Gold (g/t)
4440	Kaol + qtz	9.4	–131	*
4440A70R5A	Kaol + qtz	10.4	–143	75.0
4440A70R5B	Kaol + qtz	11.8	–152	75.0
4570CN0	Kaol + qtz	13.8	–105	44.0
4570ES3BC	Kaol + qtz	9.3	–143	8.3
4570Bsouth3TC	Kaol + qtz	15.0	–112	25.0
4640DN20	Kaol + qtz	11.0	–100	12.1
4700ES20L6+65ft	Kaol + qtz	4.5	–94	59.2
4700ES20LG(HWflt)	Kaol + qtz	12.3	–130	16.2
4770E20	Kaol + qtz	14.4	–100	*
4835 (CA32)	Kaol + qtz	7.4	–137	*
4890D20(CA26)	Kaol + qtz	12.8	–96	*

Abbreviations: Kaol = kaolinite, qtz = quartz; * = within orebody
[1] Sample numbers reflect approximate mine grid elevations, in feet, for each level

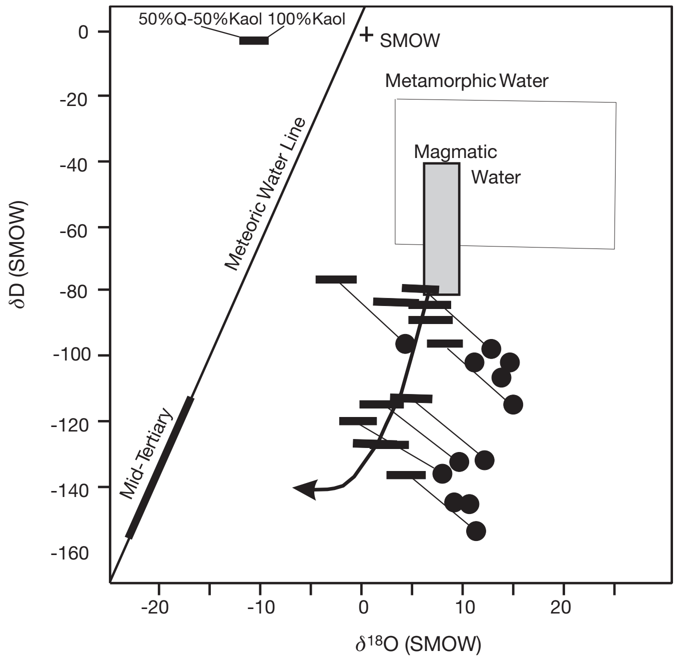

FIG. 21. Kaolinite isotopic data from Deep Star, Nevada, showing the analytical results from Table 2 (filled circles) with tie lines to water compositions (horizontal bars) in equilibrium with kaolinite at 200°C (calculations based on fractionation data from Sharp and Kirschner, 1994; Gilg and Sheppard, 1996; Sheppard and Gilg, 1996). Due to the presence of quartz impurity, tie lines reflect a water in equilibrium with 100 percent kaolinite (right end of bar) to 50 percent quartz-50 percent kaolinite (left end of bar). The upper cluster of kaolinite isotopic data comes from samples collected along the Hangingwall fault whereas the lower grouping represents samples from the eastern margin of the Deep Star orebody along the Deep Star fault.

Analyses of kaolinites for hydrogen isotopes were performed using a EuroVector elemental analyzer interfaced to a Micromass IsoPrime stable isotope ratio mass spectrometer, using a glassy carbon-packed alumina reactor at 1,300°C (modified after Koziet, 1997; Hilkert et al., 1999). The kaolinite analyses were performed at the Nevada Stable Isotope Laboratory, Mackay School of Mines, University of Nevada-Reno.

The kaolinite data form two distinct groupings with ranges of δD between –94 to –112 per mil and –130 to –152 per mil (Fig. 21). Whereas the data plot near the "kaolinite line," no supergene effects are present within the Deep Star mine. The isotopic composition of water in equilibrium with them was calculated at 200°C—a temperature that is consistent with many Carlin-type deposit fluids (Hofstra and Cline, 2000; T. B. Thompson, unpubl. data, 2002). Tie lines from the kaolinite ratios to a line representing the fluid in equilibrium with each kaolinite sample are shown. The heavy horizontal bars represent equilibrium fluid compositions for samples that consist of 100 percent kaolinite, at the right, and a mixture of 50 percent quartz and 50 percent kaolinite, at the left. The upper cluster of kaolinite isotopic data comes from samples collected along the Hangingwall fault whereas the lower grouping represents samples from the eastern margin of the Deep Star orebody along the Deep Star fault. The high-grade portions of the orebody are associated with the Hangingwall fault as is the most intense kaolinite-quartz-marcasite alteration. As can be seen from the diagram (Fig. 21), the fluids range from near the magmatic water field for those near the center of the Deep Star orebody along a mixing path toward exchanged mid-Tertiary meteoric water as represented by the fluids near the eastern orebody margin.

Discussion and Conclusions

Brittle faults have strong control on the distribution of ore and were clearly the primary ore-fluid conduits at Deep Star, as inferred for other Carlin trend deposits (Teal and Jackson, 1997). A structural framework for the Deep Star deposit was constructed by incorporating the results of other recent research (Ressel et al., 2000; P. Lewis, writ. commun., 2001; T. Leach, written commun., 1999) including petrography and isotopic dating of Eocene igneous rocks and geochemical and hydrothermal alteration zonation to delineate better the conditions of ore formation. The resulting interpretation uses as its basis the temporal relationship between mineralization and Eocene magmatism (Hofstra et al., 1999; Ressel et al., 2000), combining the known regional far-field stress (west-northwest-directed extension) during late Eocene time (Seedorff, 1991).

The Gen-Post fault system constitutes a long-lived, regional-scale structural zone, which represents the shallow manifestation of a crustal-scale discontinuity underlying the northern Carlin trend. Gold mineralization occurred relatively late in its history. Deep Star formed in a fault zone that experienced three or more episodes of oblique, strike-slip shear. The deposit is situated in an inherited structural domain different from that of most other gold deposits in the northern Carlin trend (Fig.1), which helps to explain the contrasting style and tenor of mineralization at Deep Star compared to that at Genesis (Schutz and Williams, 1995) or Carlin underground (R. Harris, written commun., 1996).

At Deep Star, mineralized northwest-striking faults have been reactivated to cut northeast-striking faults; however, at Genesis and Post, northwest-striking faults are shown to be older, reactivated faults by the presence of Jurassic lamprophyre dikes and crosscutting relations. Older northwest-striking faults at Deep Star (e.g., Pegasus) are believed to be contemporaneous with the northwest-striking fault set intruded by lamprophyre dikes at Genesis and Post. Further evidence that northwest-striking faults are older is demonstrated by trace element distributions. Gold and trace element patterns at the deposit scale are interpreted to reflect the location of fluid pathways. Dominant fluid flow, as shown by the distribution of low level gold, was vertical; however, secondary horizontal flow from east-southeast to west-northwest crosscuts the dominant north-striking Gen-Post fault system. The northwest-striking Hangingwall fault and the Pegasus fault exhibit controls on mineralization at the deposit scale but have not been traced west of the Gen fault or east of the Deep Star fault. Nevertheless, patterns within the geochemistry suggest that at least fractures of this orientation persist beyond the Gen-Post fault corridor and were important conduits for migrating fluids.

The FN-Royalty portion of the orebody is characterized by multiple, anastomosing, duplexed, shallow-dipping structures oriented subparallel to bedding. Boudinage structures are evident at the rib scale (1–5 m), suggesting that they may have formed to accommodate dextral movement along the Gen-Post fault system or that they represent earlier thrust faults which were later reactivated in a normal sense.

Numerous processes acted in concert, both prior to, and as part of the mineralizing system, resulting in the breccia textures now preserved in the ore. Mesozoic and earlier tectonic disruption associated with wrench faulting along the Gen-Post fault zone, characterized by high fracture density and steeply dipping, closely spaced structures, most likely acted as a nucleus for dissolution and collapse brecciation. Partial carbonate dissolution and collapse of calc-silicate, skarn, and marble, with subsequent hydrothermal replacement, led to multiple overprinting breccia types, ranging from primary sedimentary, through simple collapse, to fluidized hydrothermal breccias. The relative volumes of replacement versus open-space vein filling or breccia matrix infill were not determined.

The preexisting, north-striking, east-dipping Deep Star fault was reactivated in a dilatant, dextral-normal oblique sense during west-northwest-directed Eocene extension and acted as a first-order control to mineralizing fluids. Kinematics deduced from the simultaneously active Deep Star fault and Northeast break were combined to approximate the local stress regime (subhorizontal sigma 3 along a 291—111° axis) at Deep Star during Eocene dike emplacement and thus, by inference, gold mineralization (Fig. 22).

Dextral-normal oblique slip along the Deep Star fault zone, as demonstrated by kinematic indicators, would have created a dilatant releasing bend along a 90-m-strike length where the Hangingwall, Golden, Stibnite, Aussie, and Deep Star faults coalesce (Fig. 8). From this point, ore fluids were able to flow upward and outward along these faults and their associated fracture or damage zones, presumably into a zone of low mean stress facilitating gold precipitation. Similarly, the steepening dip of the Deep Star fault at the economic bottom of the deposit (Fig. 9) would create dilatancy below and restriction above this level, given the normal component of slip. This dilatancy is inferred to have focused upward-migrating ore fluids to this point and then along the path of least resistance into the footwall of the fault.

Hydrothermal fluids introduced during the Eocene mineralizing event originated at depth immediately east-southeast of the deposit within the Deep Star-Post fault corridor. As they ascended more or less vertically, they moved through the Deep Star breccia and exited immediately north of the deposit in the footwall of the Deep Star fault. Above the deposit, the fluid pathways flared out to the west in a west-northwest direction above the deposit.

The vertical plume is zoned laterally in relation to the ore deposit, probably reflecting evolution of the system (Fig. 19). Decarbonatization affected the Popovich Formation, the hanging wall to the Deep Star fault, but is also postulated to have contributed to collapse in the ore host breccia, as indicated by depletion in Ca, Mg, Ba, and Sr. High-grade gold was deposited in the Deep Star breccia, along with As, Sb, Hg, Tl, W, Zn, and Ag, presumably as solid solution substitution into arsenian pyrite rims. Within the Gen-Post fault corridor east of and above the orebody, Fe, Mn, Co, Ni, P, Cu,

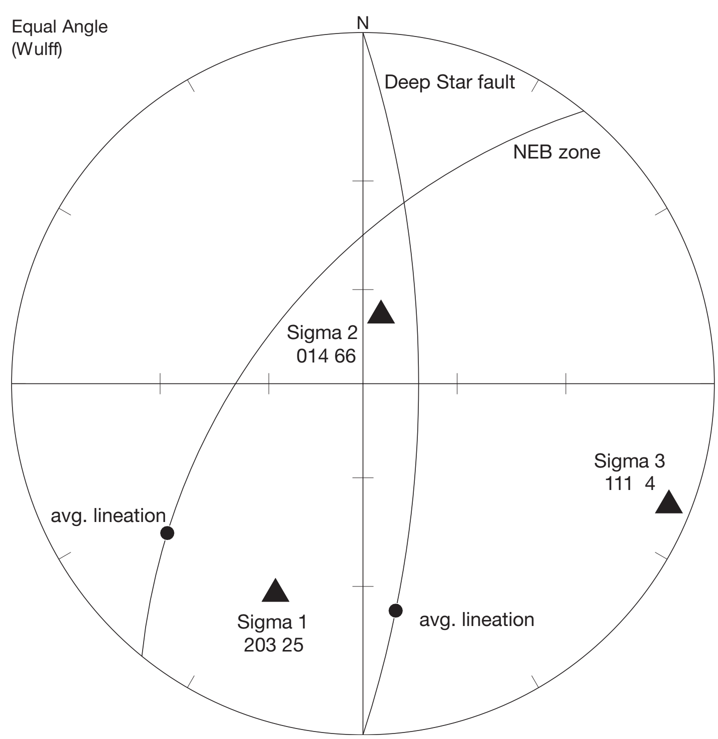

FIG. 22. Lower hemisphere equal angle projection showing local stress field at Deep Star, Nevada, estimated using representative orientations and slickenlines for the Deep Star fault and the Northeast break zone. The average slickenline for the Deep Star fault shown here is postulated to represent the earlier of two displacement events recorded, which occurred approximately synchronously with late Eocene rhyolite intrusion and gold mineralization. The resulting sigma 3, or least principal stress direction, is correlative with regional Eocene extension trending west-northwest–east-southeast (Seedorf, 1991).

Mo, U, and V were deposited in a variety of different mineral phases including Fe carbonate minerals, apatite, and pyrite. Lead and Bi were deposited within this same area and east of the Post fault in the Little Boulder Basin stock, although their timing relative to gold deposition is unclear. The deposition of all of these elements overprinted the Vinini Formation cherts above the deposit leaving an anomalous trail that is still evident 300 m above the Deep Star deposit.

Hydrothermal alteration associated with Carlin-type deposits resulted in carbonate dissolution and deposition of fine-grained quartz, pyrite, and various clays (e.g., kaolinite, illite, smectite). This also holds true at Deep Star as shown by petrographic and XRD analyses that tie the gold mineralization to the quartz-kaolinite alteration event. Further, this work has shown that white mica, or sericite, from earlier alteration events is unrelated to the Eocene gold episode.

Mineralized and unmineralized Eocene rhyolite dikes, the latter dated at 38 Ma, were emplaced into the active north-striking Gen fault and provide a minimum age for gold mineralization. Sinistral normal slip on northeast-striking rhyolite dike contacts in the Northeast break zone—dikes compositionally similar to those dated in the Gen fault but from within the orebody—is consistent with regional west-northwest-directed extension during the Eocene. Changes in the strike direction of 40 to 38 Ma dikes, from northeast to north (the K and Anne dikes at Genesis, Fig. 11, and the X dike at Deep Star, Fig. 4), as they approach the Gen fault, demonstrate a similar refractionlike geometry suggestive of synkinematic emplacement. The Gen and Deep Star faults locally were filled with rhyolite where they intersected the north- to northeast-striking dikes, which may have been emplaced into actively propagating fractures. The presence of quenched, glassy margins and the fine-grained texture of the rhyolite dikes imply a shallow depth of formation for the Deep Star deposit, which we assert to have been within 1 or 2 km of the paleosurface (see also, Ressel et al., 2000). Additionally, northeastern Nevada has been an area of high heat flow since Eocene time (Seedorf, 1991), resulting in high geothermal gradients.

Kaolinite δD and $\delta^{18}O$ data indicate that the gold-mineralizing fluids originated from either a magmatic or possibly deep metamorphic source. Fluids range from near the magmatic water field for those near the center of the Deep Star orebody along a mixing path toward exchanged mid-Tertiary meteoric water as represented by the fluids near the eastern orebody margin.

Postore displacement is indicated by sheared, fractured, broken, and displaced ore at Deep Star and represents the local manifestation of further pulses of extension which continue to the present (Seedorf, 1991). With the onset of supergene weathering, gold from the exit plume was mobilized and redeposited in the oxide zone immediately above the redox boundary within the Goldstrike intrusion. This style of mineralization is represented in several small oxide deposits including Pancana, Lost Pancana, and 5-0 (Fig. 1).

Acknowledgments

We would like to thank the Newmont Mining Corporation for allowing us to publish this work. This paper is the result of many years of mapping and research by numerous Newmont geologists, university researchers, and outside consultants. We gratefully acknowledge Diana Neef and Jeanette Hunter for drafting the figures. The quality of early versions of the manuscript was improved by the comments of Margie Lane and Steve Garwin. We would also like to thank the *Economic Geology* reviewers, Al Hofstra, Ted Theodore, and Ernie Anderson for their helpful comments.

REFERENCES

Altamirano-Morales, C., 1999, Structural control and alteration at the Deep Star deposit, Eureka County, Nevada: Unpublished M.Sc. thesis, Reno, University of Nevada–Reno, 78 p.

Altamirano, C., and Thompson, T.B., 1999, Structural geology and hydrothermal alteration associated with the Deep Star orebody, northern Carlin trend, Nevada: Ralph J. Roberts Center for Research in Economic Geology Annual Research Meeting, University of Nevada, Reno, January 7–8, 1999, Programs and Reports, 20 p.

Arehart, G.B., Foland, K.A., Naeser, C.W., and Kessler, S.E., 1993a, The $^{40}Ar/^{39}Ar$, K/Ar, and fission-track geochronology of sediment-hosted disseminated gold deposits at Post-Betze, Carlin trend, northeastern Nevada: ECONOMIC GEOLOGY, v. 88, p. 622–646.

Arehart, G.B., Chryssoulis, S.L., and Kesler, S.E., 1993b, Gold and arsenic in iron sulfides from sediment-hosted disseminated gold deposits: Implications for depositional processes: ECONOMIC GEOLOGY, v. 88, p. 171–185.

Armstrong, R.L., 1968, Sevier orogenic belt in Nevada and Utah: Geological Society of America Bulletin, v. 83, p. 273–287.

Bettles, K.H., 1989, Gold deposits of the Goldstrike mine, Carlin trend, Nevada: Society of Mining Engineers Annual Meeting, Las Vegas, Nevada, February 27–March 2, 1989, Preprint 89–158, 14 p.

Christensen, O.D., Knutsen, G.C., and Ekburg, C.E., 1987, Disseminated gold deposits of the Carlin trend, Eureka and Elko Counties, Nevada: Society of Mining Engineers Annual Meeting, Denver, Colorado, February 24–27, 1987, Preprint 87–84, 7 p.

Clayton, R.N., and Mayeda, T.K., 1963, The use of bromine pentafluoride in the extraction of oxygen from oxides and silicates for isotopic analysis: Geochemica et Cosmochimica Acta, v. 27, p. 42–52.

Cline, J.S., 2001, Timing of gold and arsenic sulfide mineral deposition at the Getchell Carlin-type gold deposit, north-central Nevada; ECONOMIC GEOLOGY, v. 96, p. 75–90.

Clode, C.H., and McComb, M., 1993, Breccias of the Deep Star gold deposit, Eureka County, Nevada, *in* Williams, C., ed., Symposium on northeastern Nevada breccia bodies: Reno, Geological Society of Nevada, p. 67–69.

Clode, C.H., Grusing, S.R., Heitt, D.G., and Johnston, I.M., 1997, The relationship of structure, alteration and stratigraphy to formation of the Deep Star gold deposit, Eureka County, Nevada: Society of Economic Geologists Guidebook Series, v. 28, p. 277–287.

Dickinson, W.R., 2001, Tectonic setting of the Great basin through geologic time: Implications for metallogeny: Geological Society of Nevada Special Publication 33, p. 27–53.

Dunbar, W., 2001, A structural model of mineralization at Deep Star, Carlin trend, Nevada: Geological Society of Nevada Special Publication 33, p. 243–261.

Emsbo, P., 1993, Geology and geochemistry of the Ordovician Vinini Formation, Roberts Mountains, Nevada: Unpublished Ph.D. thesis, Golden, Colorado School of Mines, 145 p.

Emsbo, P., Hofstra, A.H., and Lauha, E.A., 2000, Jurassic auriferous polymetallic mineralization at the Goldstrike mine, Carlin trend, Nevada [abs.], *in* Cluer, J.K., Price, J.G., Struhsaker, E.M., Hardyman, R.F., and Morris, C.L., eds., Geology and ore deposits 2000: The Great Basin and beyond: Abstracts with Programs: Reno, Geological Society of Nevada, p. B2.

Emsbo, P., Hofstra, A.H., Park, D., Zimmerman, J.M., and Snee, L.W., 1996, A mid-Tertiary age constraint on alteration and mineralization in igneous dikes on the Goldstrike property, Carlin trend, Nevada [abs.]: Geological Society of America Abstracts with Programs, v. 28, no. 7, p. A476.

Emsbo, P., Hutchinson, R.W., Hofstra, A.H., Volk, J.A., Bettles, K.H., Baschuk, G.J., and Johnson, C.A., 1999, Syngenetic gold on the Carlin trend: Implications for Carlin-type deposits: Geology, v. 27, p. 59–62.

Fleck, R.J., Theodore, T.G., Sarna-Wojcicki, A., and Meyer, C.E., 1998, Age and possible source of air-fall tuffs of the Miocene Carlin Formation, northern Nevada: U.S. Geological Survey Open-File Report 98–338, p. 176–192.

Fleet, M.E., and Mumin, A.H., 1997, Gold-bearing arsenian pyrite and marcasite and arsenopyrite from Carlin trend gold deposits and laboratory synthesis: American Mineralogist, v. 82, p. 182–193.

Gilg, H.A., and Sheppard, S.M.F., 1996, Hydrogen isotope fractionation between kaolinite and water revisted: Geochimica et Cosmochimica Acta, v. 60, p. 529–533.

Heitt, D.G., 2000, A summary of Newmont's reserve and discovery history on the Carlin trend 1965-1998: Geological Society of Nevada 2000 Field Trip Guidebook 7, p. 87–92.

Hilkert, A.W., Douthitt, C.B., Schlüter, H.J., and Brand, W.A., 1999, Isotope ratio monitoring gas chromatography/mass spectrometry of D/H by high temperature conversion isotope ratio mass spectrometry: Rapid Communications in Mass Spectrometry, v. 13, p. 1226–1230.

Hofstra, A.H., and Cline, J.S., 2000, Characteristics and models for Carlin-type gold deposits: Reviews in Economic Geology, v. 13, p. 163–220.

Hofstra, A.H., Snee, L.W., Rye, R.O., Folger, H.W., Phinisey, J.D., Loranger, R.J., Dahl, A.R., Naeser, C.W., Stein, H.J., and Lewchuk, M., 1999, Age constraints on Jerritt Canyon and other Carlin-type gold deposits in the western United States: Relationship to mid-Tertiary extension and magmatism: ECONOMIC GEOLOGY, v. 94, p. 769–802.

Ketner, K.B., 1977, Late Paleozoic orogeny and sedimentation, southern California, Nevada, Idaho, and Montana, *in* Stewart, J.H., Stevens, C.H., and Fritsche, A.E., eds., Paleozoic paleogeography of the western United Stataes: Society of Economic Paleontologists and Mineralogists, Pacific Section, Pacific Coast Paleogeography Symposium, 1st, Los Angeles, April 22, p. 363–369.

Koziet, J., 1997, Isotope ratio mass spectrometric method for the on-line determination of oxygen-18 in organic matter: Journal of Mass Spectrometry, v. 32, p. 103–108.

Kuehn, C.A., and Rose, A.W., 1992, Geology and geochemistry of the wall-rock alteration at the Carlin gold deposit, Nevada: ECONOMIC GEOLOGY, v. 87, p. 1697–1721.

Mortensen, J.K., Thompson, J.F.H., and Tosdal, R.M., 2000, U-Pb age constraints on magmatism and mineralization in the northern Great basin, Nevada, *in* Cluer, J.K., Price, J.G., Struhsaker, E.M., Hardyman, R.F., and Morris, C.L., eds., Geology and ore deposits 2000: The Great basin and beyond. Symposium proceedings: Reno, Geological Society of Nevada, p. 419–438.

Newmont Gold Company, 1996, Press release of October 22, 1996: Denver, Colorado, 1 p.

Norby, J.W., and Orobona, M.J.T., 2002, Geology and mineral systems of the Mike deposit, Eureka County, Nevada, *in* Thompson, T.B., Teal, L., and Meeuwig, R.O., eds., Gold deposits of the Carlin trend: Nevada Bureau of Mines and Geology Bulletin no. 111, p. 143–167.

Orobona, M.J.T., 1996, Structural setting of the Blue Star subdistrict: Implications for origin of the Carlin trend, Eureka County, Nevada: Unpublished M.Sc. thesis, Kingston, Ontario, Canada, Queen's University, 152 p.

Radtke, A.S., and Dickson, F.W., 1974, Genesis and vertical position of fine-grained disseminated replacement-type gold deposits in Nevada and Utah: IAGOD Symposium, 4th, Varna, Bulgaria, Proceedings, v. 1, p. 71–78.

Ressel, M.W., Noble, D.C., Henry, C.D., and Trudel, W.S., 2000, Dike-hosted ores of the Beast deposit and the importance of Eocene magmatism in gold mineralization of the Carlin trend, Nevada: ECONOMIC GEOLOGY, v. 95, p. 1417–1444.

Roberts, R.J., 1960, Alignment of mining districts in north-central Nevada: U.S. Geological Survey Professional Paper 400–B, p. B17–B19.

Roberts, R.J., Hotz, P.E., Gilluly, J., and Ferguson, H.G., 1958, Paleozoic rocks of north-central Nevada: American Association Petroleum Geologists Bulletin, v. 42, p. 2813–2857.

Rodriguez, B.D., 1997, Deep regional resistivity structure across the Carlin trend: Society of Economic Geologists Guidebook Series, v. 28, p. 39–45.

Schutz, L., and Williams, C., 1995, Gold mineralization in the Blue Star/Genesis mine, Eureka County, Nevada, *in* Craig, S., ed., Structural geology of the Carlin trend: Geological Society of Nevada Field Trip Guidebook, April 7–9, 1995, p. 167–175.

Seedorf, E., 1991, Magmatism, extension, and ore deposits of Eocene to Holocene age in the Great basin—mutual effects and preliminary proposed genetic relationships, *in* Raines, G.L., Lisle, R.E., Schafer, R.W., and Wilkinson, W.H., eds., Geology and ore deposits of the Great basin. Symposium proceedings: Reno, Geological Society of Nevada and U.S. Geological Survey, p. 133–178.

Shallow, L.J., 1999, Refractory ores at the Rain mine, Elko County, Nevada: Structural controls, wallrock alteration, petrography, and geochemistry: Unpublished M.Sc. thesis, Reno, University of Nevada, 150 p.

Sharp, Z.D,. and Kirschner, D.L., 1994, Quartz-calcite oxygen isotope thermometry: A calibration based on natural isotopic variations: Geochimica et Cosmochimica Acta, v. 58, p. 4491–4501.

Sheppard, S.M.F., and Gilg, H.A., 1996, Stable isotope geochemistry of clay minerals: Clay Minerals, v. 31, p. 1–24.

Silberling, N.J., and Roberts, R.J., 1962, Pre-Tertiary stratigraphy and structure of northwestern Nevada: Geological Society of America Special Paper 72, 58 p.

Simon, G., Kesler, S.E., and Chryssoulis, S.L., 1999, Geochemistry and textures of gold-bearing arsenian pyrite, Twin Creeks, Nevada: Implications for deposition of gold in Carlin-type deposits: ECONOMIC GEOLOGY, v. 94, p. 405–421.

Teal, L., and Jackson, M., 1997, Geologic overview of the Carlin trend gold deposits and descriptions of recent deep discoveries: Society of Economic Geology Newsletter, no. 31, 14 p.

Theodore, T.G., Kotlyar, B.B., Singer, D.A., Berger, V.I., Moring, B.C., and Cluer, J.K., 2000, Rock geochemistry in the Tuscarora Mountains, northern Carlin trend, Nevada: U.S. Geological Survey Open-File Report 00–402, 115 p.

Thorman, C.H., Ketner, K.B., and Peterson, F., 1990, The Elko orogeny-Late Jurassic orogenesis in the Cordilleran miogeocline [abs.]: Geological Society of America Abstracts with Programs, v. 22, no. 3, p. 88.

——2000, The Elko orogeny, Nevada-Utah—a major tectonic event with minor mineralization [abs.], *in* Cluer, J.K., Price, J.G., Struhsaker, E.M., Hardyman, R.F., and Morris, C.L., eds., Geology and ore deposits 2000: The Great basin and beyond. Abstracts with programs: Reno, Geological Society of Nevada, p. A14.

Wooden, J.L., Tosdal, R.M., and Kistler, R.W., 1997, Pb and Sr isotopic mapping of crustal structure in the northern Great basin: Society of Economic Geologists Guidebook Series, v. 28, p. 47–51.